Masteroppgave

NTNU
Norges teknisk-naturvitenskapelige universitet
Fakultet for ingeniørvitenskap
Institutt for energi- og prosessteknikk

Marie Hestetræet

Marine Lobe Pumps: A CFD Study on Performance and Impact on Aquatic Life

Masteroppgave i Energi og Miljø
Veileder: Pål-Tore Storli
Medveileder: Luiz Henrique Accorsi Gans
September 2023

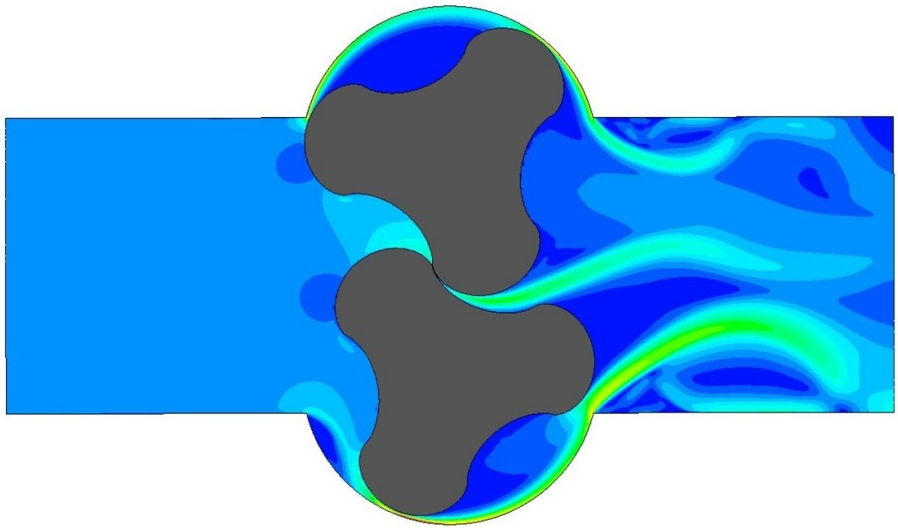

NTNU
Kunnskap for en bedre verden

Marie Hestetræet

Marine Lobe Pumps: A CFD Study on Performance and Impact on Aquatic Life

Masteroppgave i Energi og Miljø
Veileder: Pål-Tore Storli
Medveileder: Luiz Henrique Accorsi Gans
September 2023

Norges teknisk-naturvitenskapelige universitet
Fakultet for ingeniørvitenskap
Institutt for energi- og prosessteknikk

NTNU
Kunnskap for en bedre verden

Acknowledgements

Completing this master's thesis would not have been possible without the guidance and expertise of several individuals to whom I extend my gratitude. First and foremost, I would like to express my appreciation to my supervisor, Pål-Tore Storli, for his guidance throughout the writing process.

Equally, my gratitude extends to my co-supervisor, Luiz Henrique Accorsi Gans, for his expertise and assistance with the simulations. His technical knowledge and attention to detail have significantly enriched the quality of this study, ensuring that the computational aspects were accurate and meaningful.

Special thanks are also due to the team at EDR&Medeso for their collaborative assistance with the simulations. Their contribution enhanced the technical robustness of this research and provided practical perspectives that enriched the overall study.

Marie Hestetræet
Trondheim, September 2023

Abstract

In this master's thesis, the fluid dynamics of a three-lobe pump with epicycloidal lobes were investigated using computational fluid dynamics (CFD) simulations. The study emphasizes assessing the pump's mechanical interactions with aquatic life, especially in marine pumped hydro storage (PHS) projects like ALPHEUS. In addition to the simulations, the thesis incorporates a literature review that explores relevant topics such as PHS, positive displacement (PD) machines, and the application of CFD techniques to these types of machinery.

For the numerical simulations, a 2D model of the pump was created and analyzed using the SST $k - \omega$ turbulence model. The mesh employed a structured grid layout combined with inflation layers, settling on a mesh size of 1.5 mm. This approach balanced computational efficiency with the detail required for reliable results. The motion of the pump's rotors within the fluid domain was simulated using the Immersed Boundary Method (IBM), with the lobes being treated as immersed solids.

Key fluid dynamics parameters, including velocity profiles, vortex formation, turbulence, and pressure distributions, were evaluated across a range of rotational speeds from 30 to 500 RPM. The results gave insight into the pump's performance and assumed effect on surrounding aquatic life. Notably, speeds up to 100 RPM seem to strike a balance between pump performance and aquatic life safety. The results offer valuable insights into the pump's mechanical performance and likely impact on aquatic life. The findings aim to contribute to ongoing efforts to design more efficient, sustainable, and fish-friendly PHS systems.

Sammendrag

I denne masteroppgaven ble fluiddynamikken i en tre-lobet pumpe med episykloidale lober undersøkt ved hjelp av numeriske strømningsberegninger. Studien vektlegger vurderingen av pumpens mekaniske interaksjoner med akvatisk liv, spesifikt i marine prosjekter for pumpet vannkraftlagring som ALPEHUS-prosjektet. I tillegg til simuleringene, inneholder oppgaven en litteraturgjennomgang som utforsker relevante temaer som pumpet vannkraftlagring, fortreningsbaserte maskiner og teknikker for numerisk strømningsberegning for slike maskiner.

For de numeriske simuleringene ble en 2D-modell av pumpen lagd og analysert ved bruk av SST $k - \omega$ turbulensmodell. Meshet bestod av en kombinasjon av strukturerte elementer og inflasjonslag, og hadde en maskestørrelse på 1.5 mm. Denne tilnærmingen ble brukt for å balansere beregningshastighet med detaljnivået som kreves for pålitelige resultater. Rotorens bevegelse i fluiddomenet ble simulert ved hjelp av den nedsenkede grensemetoden, der lobene ble behandlet som nedsenkede faste materialer.

De viktigste fluiddynamiske parameterne, inkludert hastighetsprofiler, virvelskapelse, turbulens og trykkfordelinger, ble evaluert for rotasjonshastigheter fra 30 til 500 RPM. Resultatet ga innsikt i pumpens ytelse og antatte påvirkning på det omkringliggende akvatiske livet. Spesielt ser hastigheter opptil 100 RPM ut til å balansere pumpens ytelse med sikkerhet for akvatisk liv. Funnene har som mål å bidra til pågående arbeid med å designe mer effektive, bærekraftige og fiskevennlige PHS-systemer.

Table of Contents

List of Figures

List of Tables

Nomenclature

a_1	Constant [-]
F_2	Blending function [-]
g	Gravitational constant [m s^{-2}]
H	Water head [m]
i	Internal energy [J]
K	Thermal conductivity [W m^{-1} K^{-1}]
k	Turbulent kinetic energy [m^2s^{-2}]
P	Mean pressure [Pa]
p	Pressure [Pa]
P_k	Turbulent kinetic energy production [m^2s^{-2}]
P_{outlet}	Outlet pressure [atm]
S_i	Source term [-]
S_M	Momentum source [-]
S_{ij}	Rate of deformation [S^{-1}]
T	Temperture [K]
t	Time [s]
U	Mean velocity vector [m s^{-1}]
u	Velocity vector in x-, y- and z-direction [m s^{-1}]

Greek letters

β^*	Constant [-]
β_2	Constant [-]
Δy	Distance to the next point from the wall [m]
δ_{ij}	Kronecker delta [-]
ϵ	Turbulent dissipation rate [m^2s^{-3}]
γ_2	Constant [-]
μ	Dynmaic viscosity [kg m^{-1} s^{-1}]
μ_t	Eddy viscosity [m^2 s^{-1}]

ν Kinematic viscosity [$m^2\ s^{-1}$]

ω Specific rate of dissipation of turbulent kinetic energy [s^{-1}]

Φ Dissipation function [-]

ρ Density [$kg\ m^{-3}$]

σ_k Constant [-]

$\sigma_{\omega,1}$ Constant [-]

$\sigma_{\omega,2}$ Constant [-]

τ_{ij} Reynolds stresses [Pa]

Acronyms

BEP Best Efficiency Point

CAD Computer-Aided Design

CFD Computational Fluid Dynamic

DNS Direct Numerical Simulation

FDM Finite Difference Method

FEM Finite Element Method

FVM Finite Volume Method

IBM Immersed Boundary Method

IMS Immersed Solid

IOPAC Inverse Offshore Pump Accumulation

LES Large Eddy Simulation

LOCS Levelized Cost Of Storage

NS Navier-Stokes

PD Positive Displacement

PHS Pumped Hydro Storage

RANS Reynolds-Averaged Navier-Stokes

RMS Root Mean Square

SPH Smoothed Particle Hydrodynamics

SST Shear Stress Transport

StEnSea Stored Energy at Sea

TSBF Transverse Structured Body Fitted Mesh

Chapter 1

Introduction

As the era of renewable energy matures, the importance of reliable and efficient energy storage is becoming progressively more crucial. The need for large-scale energy storage systems becomes unavoidable with the steady rise of intermittent renewable energy sources, such as solar and wind. These systems must capably store surplus energy during periods of low demand and promptly distribute it during peak consumption times. PHS, known for its high efficiency and long life span, is a primary candidate for addressing these challenges. Yet, traditional PHS systems present their limitations. These systems rely heavily on significant elevation differences between upper and lower reservoirs, which restricts their application in regions with minimal elevation differences.

Emerging as an inventive solution to the limitations of traditional PHS, low-head PHS using seawater is gaining attention. The ALPHEUS project exemplifies this approach, employing lobe pumps for seawater-based PHS. With their assumed fish-friendly properties, lobe pumps seem well-suited to this purpose. Lobe pumps, categorized as PD pump-turbines, diverge significantly from traditional pump-turbines like Francis or Kaplan turbines. Their unique design and slower rotational speed could minimize harm to aquatic life. For the remainder of this thesis, the term pump-turbine will be simplified and referred to solely as pump.

Employing lobe pumps in seawater PHS systems presents additional benefits. Renowned for their durability, reliability, and extensive operational lifespan, lobe pumps are excellent candidates for repetitive operation in energy storage applications. Their high efficiency across a broad range of flow rates and heads [6] provides design and operational flexibility, making them a promising choice for large-scale energy storage in coastal regions.

The lack of suitable sites for traditional PHS is one of the reasons why low-head PHS using seawater is gaining attention. Finding locations with high elevations and large water bodies is often challenging and restricted in many areas. In contrast, seawater-based PHS can function in coastal regions with relatively minor differences in height between sea level and the upper reservoir. This allows the potential exploration of coastal areas for energy storage, which offers advantages such as reduced land use and minimized environmental impacts.

Ultimately, the need for reliable and efficient energy storage solutions is increasingly vital in the era of renewable energy. Low-head PHS using seawater, as proposed in the ALPHEUS project, presents a promising approach to overcome the restrictions of traditional PHS in regions with minimal elevation differences. With their assumed fish-friendly characteristics, lobe pumps could promote sustainable and environmentally conscious energy storage solutions.

1.1 Objective

The main objective of this master's thesis is to perform CFD simulations using Ansys CFX, to evaluate pump performance in combination with the evaluation of how a lobe pump can impact

surrounding aquatic life, particularly fish. This study is conducted in the context of seawater applications, which has become an important focus for initiatives like the ALPHEUS project.

Two preliminary steps are planned to set the stage for these CFD simulations. The first is a comprehensive literature review covering PHS, PD machines, and existing CFD techniques relevant to the analysis of PD machines. This review aims to provide the necessary theoretical background to guide the subsequent design and simulation phases, ensuring that they are grounded in the current state of the art.

The second preliminary step involves using Computer-Aided Design (CAD) software to create the lobe pump design. This design will serve as the basis for the CFD simulations, which constitute the main focus of this thesis. While the pump is intended for seawater applications, the design considerations will center on its efficacy in handling water in a general sense, laying a solid foundation for in-depth CFD analyses to follow.

Once the CAD design is completed, the thesis will zero in on its central objective: executing CFD simulations to explore various flow characteristics, such as velocity and pressure, and most critically, interpreting the results to assess the pump's potential impact on aquatic life, notably fish. These simulations are not just an evaluation of the pump's technical attributes but are aimed at performing an essential environmental assessment.

The core of this thesis lies in interpreting the CFD simulation results, especially in terms of how the pump operation might affect the surrounding fish. With marine ecosystems being extremely sensitive to environmental changes, it becomes imperative to design a mechanically sound and ecologically responsible system.

In summary, the thesis aims for a dual contribution: advancing the field's understanding of PD machines, particularly lobe pumps, within the framework of PHS systems and seawater contexts such as those associated with the ALPHEUS project. At the same time, the thesis aims to highlight the importance of considering environmental responsibility in engineering practices. Through a focus on CFD analyses, the research seeks to provide a balanced evaluation of a lobe pump, examining its mechanical behavior and potential ecological impact. This approach addresses the concurrent challenges of effective engineering design and environmental sustainability.

1.2 Literature Review

Energy storage systems have a crucial role in ensuring the stability and reliability of power grids. PHS offers a reliable and sustainable solution among the various energy storage technologies. PHS has been the subject of research and development for over a century, with a recent shift towards low-head PHS. This shift is mainly due to the global trend towards renewable energy sources. In addition to that, many high-head PHS sites are no longer viable. As the reliance on renewable energy sources continues to grow, the demand for increased energy storage capacity increases. Low-head PHS presents a viable answer to this challenge.

This literature review examines the current state of the art in PHS and PD machines, focusing mainly on low-head PHS and lobe pumps. It also intends to investigate the CFD techniques employed to enhance these machines' design and performance. The following literature review is mainly built upon the project work "Numerical setup for a positive displacement reversible pump-turbine machine" by Hestetræet [4].

1.2.1 Pumped Hydro Storage

The global energy landscape is rapidly transforming, moving towards renewable resources and away from fossil fuels. This is mainly due to increasing awareness of the negative environmental impacts of traditional energy sources and the need to reduce greenhouse gas emissions. However, the reliance on energy sources such as wind and solar power, dependent on nature's forces and cannot be regulated according to demand, poses unique challenges. To counter these challenges

and minimize energy waste, there is a need to store energy produced from these sources for future use.

PHS is a widely used technology for energy storage. Water is pumped from a lower reservoir to an upper reservoir using low-cost electric power, such as electricity generated from wind turbines during off-peak hours. When energy is needed, the water is released from the upper reservoir, passing through a turbine and generating electricity. According to the International Renewable Energy Agency, PHS is expected to have a significant market presence, anticipated to reach 325 GW by 2030 [7].

Compared to other energy storage technologies, PHS has several advantages, including high efficiency, large capacity, and prolonged lifespans. Some hydropower plants have been operating for over 120 years. This longevity gives PHS a considerable advantage over battery systems, which generally have a lifespan of just 15 years [2].

However, PHS systems also have some disadvantages, with one key downside being their heavy reliance on topography and elevation differences. Consequently, regions with flat topographies are unsuitable for traditional PHS systems. A new form of PHS known as low-head PHS is emerging in response to this limitation. Defined as having less than 30 meters of elevation difference between upper and lower reservoirs, low-head PHS is expected to broaden storage opportunities, particularly for flat regions like the Netherlands and Denmark.

Due to its high efficiency, quick response times, and energy and power capacity, PHS has become an attractive research area. Hoeffstaedt *et al.* states that this motivates the use of PHS, in addition to the low levelized cost of storage (LCOS). LCOS measures the lifetime average cost of power production for an electricity plant. However, the low LCOS only applies to high-head PHS, and low-head PHS has received limited attention due to this [2]. According to Hoeffstaedt *et al.*, the high LCOS for low-head PHS is due to large civil structures, expanded machinery, and lower round-trip efficiencies. The authors also state that the expected demand for energy balancing will likely justify the higher LCOS. In addition, the development of low-head PHS technologies might lower the LCOS.

To enhance low-head PHS's economic and technical competitiveness, Hoeffstaedt *et al.* identified three critical areas for improvement: pump-turbine design and configuration, grid integration, and electrical machines and control [2].

Progress in the PHS field has been substantial, with the introduction of deep-sea PHS technology being a noteworthy development. The Stored Energy at Sea (StEnSea) project, an initiative by Fraunhofer IEE, involves submerging a hollow sphere into deep waters, from 600 m to 800 m, to store energy using static water pressure. The sphere houses a pump-turbine that pumps water out to store energy and generates energy when water refills the sphere [8]. A study by Hanh *et al.* [9] found that StEnSea's ability to store electricity and balance power services is comparable to traditional PHS and compressed-air energy storage systems. The report also noted that if operating costs are the same, the StEnSea concept has advantages such as its closer proximity to power generation sites like offshore wind farms and its lower environmental impact.

The potential of the StEnSea project was further validated by a pilot test conducted in Lake Constance, Germany, using a 3 m diameter sphere with a fully automated system. The sphere was installed and tested at a depth of 100 m for four weeks during the winter of 2016/2017 and was successful in demonstrating that this technology has the potential to be a vital part of the future energy system. Despite the project's success, simulations recommended testing a 1:3 scale prototype at a full depth of 700 m before proceeding with a full-scale prototype [7].

Using seawater for PHS was first tested at the Okinawa Yanbaru Seawater Pumped Storage Power Station. Although the plant was completed in 1999, it was eventually demolished in 2016 as it was not profitable. This project demonstrated the feasibility of seawater PHS, but also highlighted the challenges it presents, such as saltwater corrosion and growth of barnacles [10].

Another concept was introduced in 2007 by De Boer *et al.*, known as the inverse offshore pump accumulation (IOPAC) station, as shown in Figure 1.1. This technology combined seawater PHS with an offshore wind power plant by placing the IOPAC station on an artificial island of dikes and

a 50 m deep reservoir. The reservoir, proposed to have a capacity of 60 GWh, was estimated to be 6 km by 10 km in size. One of the uncertainties for this project is leakage into the surroundings. The report's findings show that the concept is technically and economically feasible [1], but the project was never built.

Figure 1.1: The inverse offshore pump accumulation station presented by De Boer *et al.* [1] in 2007

In 2014, the Taiwan Integrated Energy Storage Island was designed following De Boer *et al.*'s concept. Although the Belgian federal government funded the iLand project in 2018, it has been delayed due to permit problems. There are currently few designs for low-head PHS systems in seawater, and none have been constructed yet [11].

The ALPHEUS project was launched in 2020 to evaluate the feasibility of low-head PHS in the North Sea, with the enclosed reservoir and the sea serving as the upper and lower reservoirs, respectively, as shown in Figure 1.2. The vertical separation between these is approximately 20 m. Seawater is pumped up from the ocean during excess electricity, while during shortages, it is released through a turbine in the enclosed reservoir to generate electricity.

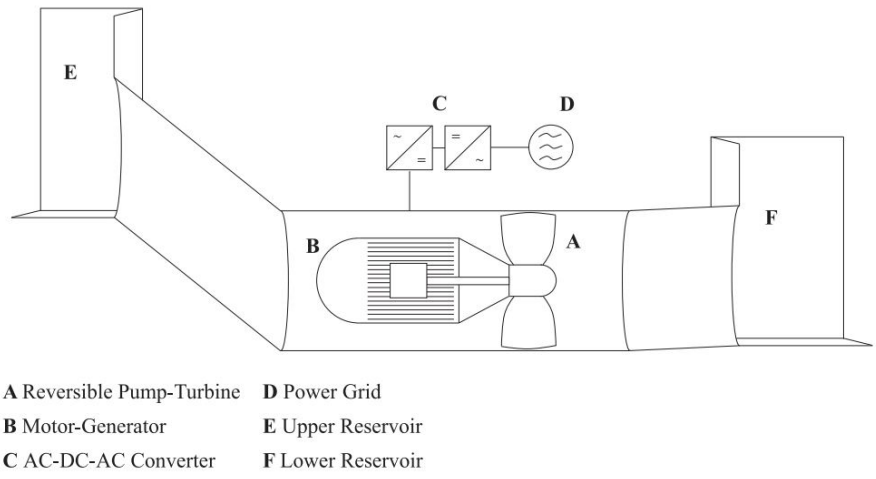

Figure 1.2: Figure of the low-head PHS concept planned for the ALPHEUS project [2]

The project's success depends on several factors, including new pump-turbine and powerhouse designs, power electronics, and sustainability considerations. Both PD machines and traditional

turbo machinery are under consideration. ALPHEUS has committed to designing new structures, reversible pump-turbines, and electrical systems to enable low-head PHS in the North Sea [11].

1.2.2 Positive Displacement Machines

PD machines operate by altering the volume of one or more enclosed chambers. When a crankshaft within the machine rotates, it alters the chamber volumes, impacting the fluid's torque or pressure. Contrary to rotodynamic machines, primarily relying on kinetic energy, PD machines exchange energy using potential energy [12]. In their book, "Positive Displacement Machines: Modern Design Innovations and Tools", Sultan and Phung enumerate several design challenges associated with PD machines. These include ensuring high manufacturing precision, using a specific geometric approach to avoid metal-to-metal contact, mitigating friction-induced losses and heat generation, preventing leakage within the working chamber, and incorporating complex control systems for machine operation. The authors indicate that available resources can address these issues despite these challenges. Further, advancements in manufacturing and material technology imply the feasibility of creating precise and complex designs of these machines at a lower cost than before.

PD pumps are a type of PD machine. Figure 1.3 illustrates some common examples. As highlighted by Jacoby [6], PD pumps present certain operational advantages under specific conditions. Regardless of changes in pressure, these pumps maintain a consistent flow rate and efficiency and adapt well to viscosity alterations. Higher viscosities can enhance the flow rate as the liquid fills the pump's gaps. A PD pump is also preferred when operating away from the best efficiency point (BEP), as it remains effective even further away from the BEP [6]. Given their low rotational speed and small shear forces, PD pumps can also handle fluids containing solids, demonstrating fish-friendly characteristics [2]. This characteristic makes them a viable contender for the ALPHEUS project, even though their traditional applications are often associated with high-head flows.

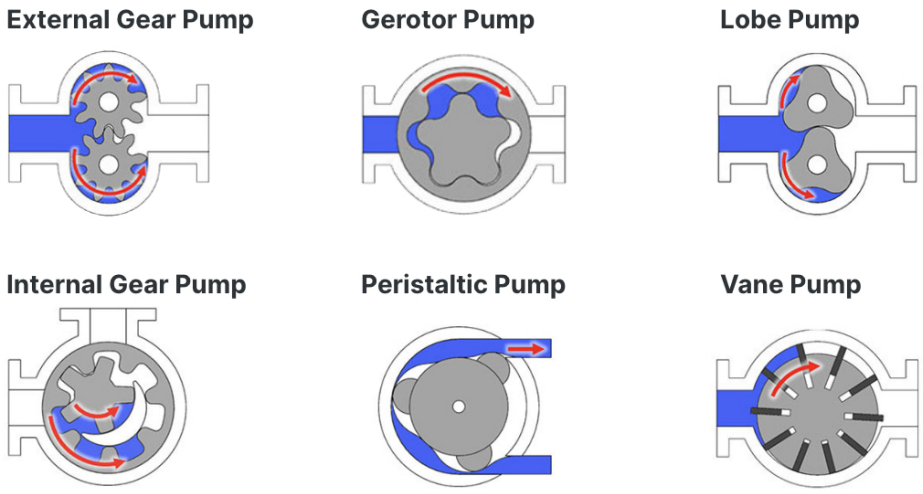

Figure 1.3: Some common positive displacement pumps

In scenarios demanding low specific speeds - characterized by high head and low flow rate conditions, PD pumps emerge as the optimal choice, as proposed by Hoffstaedt *et al.*[2]. Water supply pipelines offer a fitting example of such a system. Sonawat *et al.* [13] explored the potential of enhancing the energy efficiency of these systems by substituting a pressure differential control valve with a multi-purpose PD turbine. This turbine would reclaim energy from hot water transportation pipelines for other applications. Their study revealed that this innovative design had an overall efficiency of 67.7%, significantly reducing CO_2 emissions.

Krampe and Ørke [14] further confirmed the viability of using PD machines for pipeline pressure

management, mirroring the findings of Sonawat and his team. Their study found that PD pumps can serve a dual role in water pipelines - facilitating in-conduit pressure management and energy recovery. Furthermore, the study demonstrated that lobe geometry could significantly enhance energy delivery efficiency and precisely regulate pressure.

Kang *et al.* [3] conducted a study to identify the impact factors in the performance of lobe pumps, a particular type of PD pump. The research compared the performance of a pump with a circular-based rotor to that with an epicycloidal-based rotor, revealing that the rotor profile significantly affects pump performance. They found that the pump with an epicycloidal rotor outperformed the circular counterpart. Additionally, the study discovered that a higher rotational speed contributes to a more stable output, while lobe pumps performing at a lower rotational speed frequently give unstable pressure heads with several pressure drop points.

As noted in Hoffstaed *et al.*'s article [2], several small-scale projects have already tested PD reversible pump-turbines for low-head PHS applications. Nevertheless, testing with real-scale prototypes is paramount to verifying their applicability in such contexts. This is a common challenge the industry faces, where limited information is available from small-scale experiments, as pointed out by Kang *et al.* [3], which can result in significant error. CFD simulations often come into play to overcome this limitation, offering a thorough understanding of the full-scale model's performance across its entire operational domain.

1.2.3 CFD Techniques for Positive Displacement Machines

CFD techniques are numerical techniques that simulate fluid flow in a system for given inlet and outlet conditions. According to Hesse *et al.* [15], CFD simulations have promising potential to be a significant part of the development of PD machines. Among the different CFD techniques applied to PD machines are the Immersed Solid (IMS) method, Moving Mesh, TwinMesh, Smoothed Particle Hydrodynamics (SPH) method, Transverse Structured Body Fitted Mesh (TSBF), and IBM.

One of the main challenges of CFD for PD machines is their complex rotating geometries, which cause a highly transient flow behavior. Schiffer [16] proposes using the IMS method to mitigate this challenge. This method places a rotating solid domain within a stationary fluid domain. However, the article notes that a suitable CFD setup must be found before the IMS method can be considered a viable solution for PD machines. The paper's numerical study reveals a divergence of about 7% between the measured and simulated results, indicating the need for further refinement. Furthermore, Schiffer flags several limitations to the IMS method, including insufficient treatment of the walls of the immersed solid, potentially leading to an underestimation of the viscous forces and torques. Hesse *et al.* [15] builds on this critique by noting that the method is limited to incompressible and single-phase flows and neglects the effects of cavitation and compressibility.

Kovacevic and Rane [17] identify further challenges in the CFD modeling of PD machines. One such challenge is the solution's conservativeness, which heavily relies on selecting an appropriate grid. A poorly chosen grid can cause the solution to fail to converge. Another obstacle lies in the trade-off between computational speed and solution precision. While segregated solvers may yield results quicker than coupled solvers, the stability of these can't always be guaranteed. Moreover, the authors highlight issues such as numerical instabilities and energy loss due to misalignment and improper equation discretization. Using normal planes in mesh generation could serve as a countermeasure for these complications.

TwinMesh, a meshing technique for PD machines by Ansys CFX Berling [15], generates hexahedral meshes for each time step to represent the constantly shifting volumes. Hesse *et al.* [15] have demonstrated through their research that simulations employing TwinMesh provide results closely aligned with experimental data, and that other meshing techniques are less accurate and less efficient.

Ansys FLUENT has also developed a Moving Dynamic Mesh Tool that models domains that change over time due to motion in the domain boundaries [3]. The model's accuracy can be significantly enhanced by setting defined inlet conditions. Various numerical studies employing Fluent and

the Moving Dynamic Mesh Tool have been conducted, including a study by Kim *et al.* [18] of a hydraulic gear pump. They found that the gap size between the rotors and casing wall to be a critical factor impacting pump capacity. Kang *et al.* [3] concluded from their study that the Moving Dynamic Mesh Tool is an efficient instrument for analyzing and testing the design for lobe pumps and emphasized the significant influence the profile of the rotors exerts on the overall pump performance.

The SPH method, mainly used for turbomachinery, has rarely been applied to PD machines, as stated by Cavazzini *et al.* [19]. The only study employing this method on a PD machine was conducted in 2003 by Prakash *et al.* [20], who simulated a lobe pump. The findings revealed the SPH method's suitability for handling flows with complex free surface behavior and flows circulating around moving objects, such as a lobe pump. However, this method has not been further utilized in any other studies related to PD machines, as indicated by Munih [21].

According to Kovacevic *et al.* [17], the TSBF method offers two meshing options: one that rotates with the rotor and a second that remains stationary with the casing, deforming in line with the rotor's surface. Regarded as the only entirely conservative method to date, the TSBF method has been applied in various numerical studies. Notably, a study by Papes and Vierendeels [22] employed this method, yielding satisfactory results despite the challenges presented by the deforming domain. These challenges were addressed using an in-house code.

The IBM, initially developed by Charles Peskin in 1972 to simulate heart-induced blood flow, is a type of CFD technique capable of simulating the action of a rotating solid domain immersed within a static fluid domain [16]. Unlike other methods, IBM allows the computational grid to diverge from the flow boundary, with solid boundaries as discrete points known as immersed boundary points. The CFD equations are then applied to these individual points, and the flow around them determines their movement [23].

In 2017, Khalili *et al.* [24] combined high-order summation-by-parts operators with IBM to simulate the flow past a circular cylinder. The simulation results yielded a strong alignment with experimental data. Another successful application of IBM is seen in Gans' 2022 study [23] that is part of the ALPHEUS project. This study utilized IBM to simulate a rotary lobe pump to identify the best design choices for the lobe pump.

The IBM is an advantageous selection for the CFD simulation of a lobe pump primarily because it can simulate complex geometries without meshing the entire domain. This has been demonstrated in Gans' previous work [23]. In situations where geometries evolve - such as in a lobe pump with rotating lobes - IBM's capabilities are particularly valuable. Moreover, it can also simulate the motion of flexible or deformable boundaries like the lobes compressing the fluid during rotation, which can prove challenging with other methods. For instance, the finite element method demands rigorous mesh refinement to capture deformable boundary motion accurately. IBM considers the rotors as immersed bodies, enabling the flow simulation around a PD pump-turbine. This approach distinguishes between cells located in the fluid of the solid and interpolates the variable values at the boundary. Consequently, the need to recompute the complete numerical mesh at each time step is eliminated, resulting in a significant reduction of computational time [23].

Chapter 2

Theory and Numerical Method

As the world continues to evolve and innovate within renewable energy sources, there's a pressing need to refine PHS technologies. Central in these advancements is the study of lobe pumps. These pumps' distinct designs and mechanisms play a crucial role in the internal fluid dynamics, and CFD is often employed as an analytical tool to understand this dynamic comprehensively. While the primary emphasis in this chapter is on the technical aspects of fluid movement and the use of CFD, the overarching goal remains to understand the potential effects of lobe pumps on aquatic life.

The following chapter covers key topics for this thesis: lobe pumps, fluid dynamics, CFD, and the numerical setup. The lobe pump section provides insight into the design and operation of these PD machines. The following fluid dynamics section offers a basic understanding of how fluids behave within these systems. The application of CFD for the simulation and analysis of these fluid flows will be presented. While the above sections present an overview of these topics, the chapter concludes with the simulation setup, highlighting the specific geometry and numerical method used in the simulations for this thesis.

2.1 Lobe Pumps

Lobe pumps are PD pumps known for their flexibility and aptitude for handling high-viscosity fluids [6]. Their unique design, characterized by revolving lobes, facilitates fluid movement through the suction, transfer, and discharge stages. Lobe pumps have emerged as a suitable choice for low-head PHS systems despite water not being a high-viscosity fluid. This is due to their assumed fish-friendly characteristics [2]. The pump does not squeeze or harm the fluid, and this operational strategy protects aquatic life as the fluid is handled gently and efficiently throughout the process.

However, the design and efficiency of a lobe pump are influenced by several factors, such as the number and shape of the lobes and their arrangement within the pump. Understanding these design elements and the principles of lobe pump operation is integral for optimizing their performance within different applications, including low-head PHS systems. This section provides an in-depth overview of lobe pumps, focusing on their principles of operation, the significance of lobe geometry and design, and their relevance to low-head PHS systems.

2.1.1 Principles of Operation

A lobe pump consists of two rotors rotating synchronized, non-contact within a casing. The lobe rotors, often driven by external gearing, spin simultaneously, ensuring that the fluid within the casing is moved smoothly and continuously [12]. The unique feature of a lobe pump is its operational simplicity and reliability. With only two moving parts, a lobe pump requires minimal maintenance, potentially leading to lower operational costs over its lifetime.

The mechanism underlying the lobe pump involves a four-phase process: suction, transfer, compression, and discharge [12]:

- **Suction Phase:** This phase initiates the operation. An expanding cavity forms as the lobes evolve away from each other at the pump's inlet. This cavity expansion creates a vacuum-like effect, drawing fluid into the pump chamber. The volume of the fluid drawn in depends on various parameters, such as the lobes' rotational speed, the pump's dimensions, and the relative pressure conditions at the pump's inlet and outlet.
- **Transfer Phase:** Once the fluid is inducted during the suction phase, the transfer phase takes over. With the lobes' continuous revolution, the fluid, now entrapped between the lobes and the pump casing, is guided from the pump's inlet to its outlet side. The fluid movement occurs spontaneously, a direct result of the unceasing rotation of the lobes.
- **Compression Phase:** As the fluid moves towards the outlet side, it undergoes a subtle compression. While this compression is generally mild, it prepares the fluid for the discharge phase. Notably, this compression process can be assumed to be gentle enough to cause minimal harm to aquatic life such as fish. However, it is crucial to consider various factors like the size and species of the fish. This thesis will not consider this as it is outside the scope.
- **Discharge Phase:** Concluding the process is the discharge phase. Here, the rotating lobes propel the fluid out of the pump through the outlet side. In this phase, the fluid's pressure surges to align with the discharge pressure parameters, ensuring the efficient transition of the fluid from the pump to its subsequent destination.

An added function of the lobe pump is its ability to function in reverse as a turbine, a mode of operation where the pump converts hydraulic energy into mechanical energy. This feature significantly adds to the versatility and efficiency of lobe pumps, allowing them to be employed in diverse settings such as PHS systems.

2.1.2 Geometry

The geometry of lobe pumps is important in their operation, efficiency, and performance. This subsection will explore the design characteristics of the lobes, covering aspects such as their size, shape, the number of lobes involved, and the spatial arrangement between them. Note that this subsection aims to give a general overview of the geometry of lobe pumps, highlighting their key elements without going into specific numerical values or design details. The exact design parameters applicable to the lobe pump geometry for this thesis will be discussed later in Section 2.3.

Lobe Size

The lobe size plays an important role when determining the overall performance of the pump system. The lobe size can become especially important in low-head PHS, which aims to move large volumes of water using as little energy as possible.

The larger the lobes, the more fluid can be displaced per rotation. With larger lobes, more space is created for fluid to flow into during the suction phase of operation, allowing a greater volume of fluid to be handled with each rotational cycle. This, in turn, results in higher flow rates, which is a key requirement for the efficient operation of low-head PHS systems. However, it is essential to consider that an increase in lobe size can also mean an increase in the overall pump size and weight, with implications for installation, operating costs, and energy efficiency. Larger lobes require a larger casing and more robust mounting systems. Regarding energy use, larger lobes require more torque to rotate, leading to higher energy requirements. Thus, finding the optimal lobe size for a specific application is a balancing act.

Moreover, the size of the lobes can also influence the pump's ability to handle solids, such as fish. Larger lobes tend to create larger spaces between the lobes as they rotate, potentially reducing the risk of injury to fish or other aquatic life.

In summary, the lobe size can significantly impact the performance of lobe pumps in low-head PHS systems. Determining the optimal size is a critical design decision that must consider various factors, including the desired flow rate, energy efficiency, pump size and weight, and environmental considerations.

Lobe Shape

The shape of the lobes will also influence the pump's operational characteristics, including flow rate, pressure, and efficiency. Lobes may have a variety of shapes depending on the specific requirements of the applications. For PHS applications, two shapes of lobes can be considered: circular-based lobes and epicycloidal-based lobes.

Circular-based lobes, as the name implies, feature a design where the lobes follow the contour of a simple circle. This simple, symmetrical design makes manufacturing easier while ensuring a steady, uninterrupted flow. These lobes generally have a consistent size and curvature across the entire lobe length, which reduces turbulence and decreases the chances of cavitation. However, despite their benefits, these lobes exhibit lower flow rates and efficiency levels than epicycloidal-based lobes, as shown by Kang *et al.* [3]. Both geometries are shown in Figure 2.1 for a two-lobe pump.

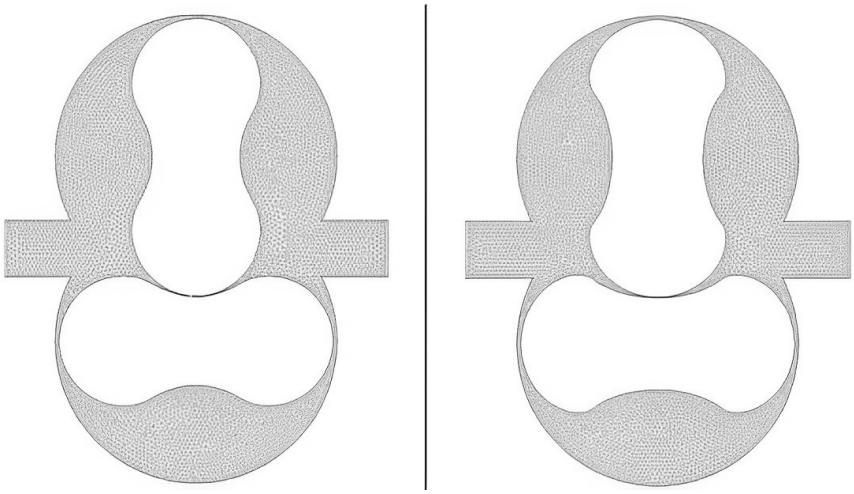

Figure 2.1: Two-lobe pump with circular lobes (left) vs. Two-lobe pump with epicycloidal lobes (right) [3]

The epicycloidal-based lobes are designed based on the principles of epicycloidal geometry. An epicycloid is a shape traced by a point on the circumference of a smaller circle rolling outside a larger fixed circle. This results in a more complex shape compared to the circle. These lobes are often used in pumps with three or more lobes. Compared to circular-based lobes, this shape offers some other benefits. One of these is that they create less pressure drop in the pump [3], which means that the pump doesn't have to work as hard to move fluid from one place to another. Epicycloidal lobes also need less suction pressure at the pump inlet to work appropriately, called having a lower net positive suction head requirement. As a result of these benefits, the epicycloidal-based lobes are considered best suited for the lobe pump utilized in a low-head PHS system.

Number of Lobes

The number of lobes is an important parameter. Lobe pumps can have different numbers of lobes, commonly two, three, or even four, depending on the specific application and operational

requirements. A two- and a three-lobe pump geometry is shown in Figure 2.2.

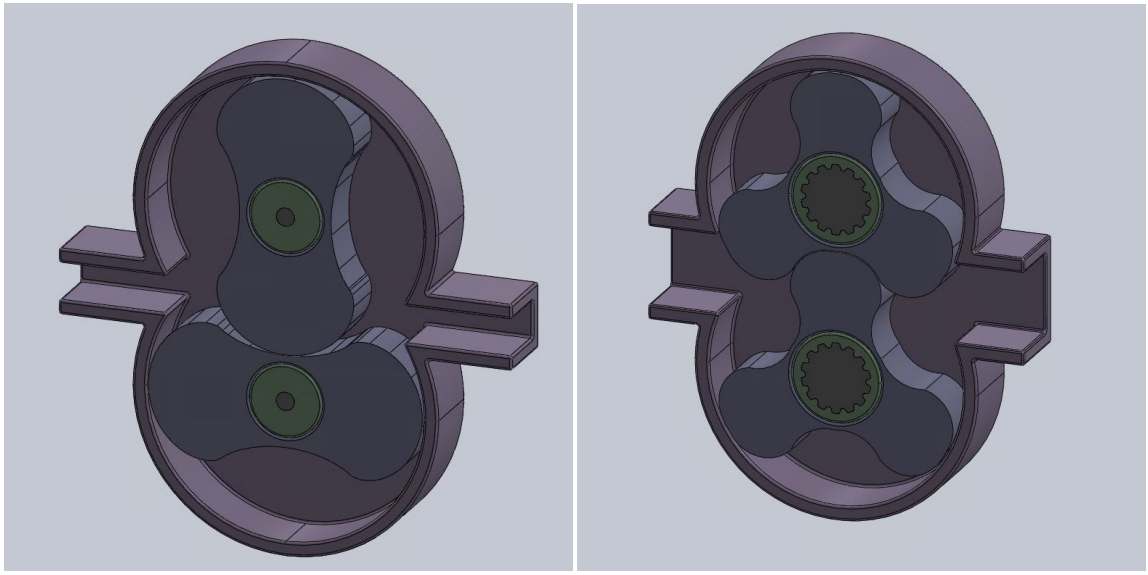

Figure 2.2: Two-lobe pump geometry (left) vs. Three-lobe pump geometry (right) [4]

While the standard two-lobe pump design is simple, it might not deliver the optimum performance for low-head PHS systems that often require large volumes of water to be moved with minimal pulsation. The two-lobe design causes more pulsation and a less uniform flow, as shown by Kang *et al.* [3], potentially affecting the system's efficiency.

Conversely, pumps with three or four lobes present an alternative. These designs yield a higher flow rate and a smoother, more uniform flow due to the increased number of lobes [3]. The smoother flow can significantly enhance the performance of low-head PHS, given the large volume of water involved. The flow rate will, in theory, increase with the number of lobes since more cavities for fluid intake are formed during each rotation.

However, adding more lobes leads to a more complex pump design, demanding careful consideration to prevent contact and subsequent wear and tear of the lobes and pump casing. The precision required in the design and manufacturing process often leads to increased costs, which must be weighed against the potential gains in system efficiency and effectiveness.

Therefore, considering the specific operational requirements, choosing between two-, three-, or four-lobe designs in low-head PHS applications must be carefully evaluated. The desired flow rate, efficiency, operational smoothness, design, and manufacturing complexities should all be factored into the decision-making process. The choice for the ALPHEUS project is a three-lobe pump geometry with epicycloidal lobes [23]. This thesis will accordingly adopt this three-lobe configuration.

Clearance Gap of Lobes

The clearance gap refers to the space between the lobes themselves and between the lobes and the casing. It is a crucial element in lobe pump design. This space is significant for several reasons, mainly concerning the pump's efficiency, the fluid's smooth flow, and preventing damage to the pump itself.

Regarding pump efficiency, the gap size directly influences the degree of slippage or backflow within the pump. Smaller gaps typically decrease the chance of backflow, leading to a more efficient pump operation. However, excessively small gaps might increase the risk of contact between the lobes and the casing, potentially causing damage or increased wear on the pump components. An optimal balance should be found between minimizing backflow and preventing mechanical contact.

The gap also plays a vital role in the fluid's smooth flow. It allows the fluid to move and be directed toward the pump outlet without creating high-pressure zones. If allowed to develop, these zones could disrupt the consistent flow of fluid and potentially lead to phenomena like cavitation, which can damage the pump's mechanism.

Another important role of the clearance gap is to prevent friction and wear between the lobes and the casing. The gap ensures that moving parts operate without directly contacting one another, thus minimizing the potential for abrasive interactions. Without this gap, components would continually rub against each other, increasing friction. This friction reduces the system's efficiency due to energy losses and accelerates the wear and tear of the parts involved. Over time, such wear can compromise the integrity and functionality of the system, leading to frequent maintenance needs or even total system failure. Therefore, the clearance gap is a protective barrier, ensuring the system's longevity by drastically reducing friction-induced wear.

Interestingly, when operating in marine environments, the presence of algae could potentially play a role in the pump's functionality. Although generally considered an inconvenience or potential damage source, algae could positively impact if conditions are met. Specifically, if a suitable gap size is chosen, algae filling the gap could potentially aid in reducing backflow and increasing the pump's efficiency. Of course, this would require a careful balancing act to avoid potential negative impacts such as increased friction or blockages.

This section has outlined the fundamental geometry of lobe pumps and highlighted the importance of key aspects such as lobe size, shape, number, and clearance gap. However, while technical considerations are crucial, it is also important to consider how the system will affect the surrounding aquatic life. The balance between engineering precision and ecological consciousness is vital, and this thesis aims to examine the fluid dynamics within the pump and interpret this into the potential impact on aquatic life, notably fish.

2.2 Fluid Dynamics

Studying how fluids move, known as fluid dynamics, is essential to science and engineering. Fluid dynamics plays a crucial role in understanding and optimizing the operation of various mechanical devices, including the lobe pump. This section will consider some central aspects of fluid dynamics: the Navier-Stokes (NS) equations, turbulence models, and vortex formation in lobe pumps.

2.2.1 The Navier-Stokes Equations

The NS equations, named after Claude-Louis Navier and Gabriel Stokes, serve as a cornerstone for understanding the movement of viscous fluids. Viscous fluids are real fluids flowing with some resistance in the opposite direction of their flow. Central to the NS equations represent the interplay between speed, pressure, temperature, and density, thereby essential in studying and modeling fluid dynamics.

The NS equations are derived from the fundamental conservation principles: the conservation of mass, Newton's second law of motion, and the first law of thermodynamics. Notably, the perfect gas equation, which establishes the relationship between pressure, temperature, and density for ideal gases, is incorporated within the energy component of these equations. Mathematically, the NS equations combine the continuity equation for mass conservation, the momentum equation representing a force balance, and the energy equation representing the balance of energy. The nonlinear partial differential equations illustrate complex fluid behavior under various conditions [25].

The following section will have aspects similar to the prior project work "Numerical setup for a positive displacement reversible pump-turbine machine" by Hestetræet [4]. This similarity arises because the previously mentioned project work was foundational to the research presented in this thesis. It should also be noted that the following equations will be presented in 3D form. Yet, in the

subsequent numerical setup and simulations, a 2D framework will be employed. The introduction of the 3D equations provides a comprehensive understanding of the underlying physics and general applicability across various geometries. By presenting the equations comprehensively, clarity and completeness are ensured, despite the shift towards 2D in the later sections.

The mass equation, often called the continuity equation, is the mathematical representation of the conservation of mass. This fundamental law states that mass can neither be created nor destroyed. In the context of fluid dynamics, it manifests as the principle that the rate at which mass enters a system must be equal to the rate at which it leaves, assuming there are no changes in mass within the system itself. The continuity equation is crucial for a fluid flowing in a lobe pump. It ensures that the mass flow rate remains constant irrespective of the changes in velocity or cross-sectional area of the pump. The mass equation is given in Equation (2.1), assuming a laminar, unsteady, compressible, and 3D flow. These assumptions also yield the momentum and continuity equations.

$$\frac{\partial \rho}{\partial t} + \operatorname{div}(\rho \mathbf{u}) = 0 \tag{2.1}$$

where ρ is density, t is the time and $\mathbf{u} = (u, v, w)$ is the velocity vector with velocities in x-, y-, and z-direction accordingly [26].

The momentum equations, derived from Newton's second law of motion, define the balance between forces acting on a fluid and the rate of momentum change within the fluid. They are written for each spatial direction - typically denoted as x, y, and z in a 3D Cartesian coordinate system. For the x-direction, the momentum equation accounts for forces due to pressure, viscous stresses, and external body forces and their influence on the rate of momentum change in the x-direction. Similarly, the y- and z-component equations account for these forces in their respective directions. These equations explain how fluid particles move under various forces, enabling the prediction of fluid flow behavior. They are particularly crucial for understanding complex flow scenarios, such as those encountered in a lobe pump, where the fluid's momentum varies significantly due to changes in direction and speed. The momentum equations are given in Equations (2.2), (2.3), and (2.4), for x-, y-, and z-momentum accordingly.

$$\frac{\partial (\rho u)}{\partial t} + \operatorname{div}(\rho u \mathbf{u}) = -\frac{\partial p}{\partial x} + \operatorname{div}(\mu \operatorname{grad} u) + S_{Mx} \tag{2.2}$$

$$\frac{\partial (\rho v)}{\partial t} + \operatorname{div}(\rho v \mathbf{u}) = -\frac{\partial p}{\partial y} + \operatorname{div}(\mu \operatorname{grad} v) + S_{My} \tag{2.3}$$

$$\frac{\partial (\rho w)}{\partial t} + \operatorname{div}(\rho w \mathbf{u}) = -\frac{\partial p}{\partial z} + \operatorname{div}(\mu \operatorname{grad} w) + S_{Mz} \tag{2.4}$$

where p is pressure, μ is dynamic viscosity and S_M is the momentum source [26].

The energy or heat equation, given in Equation (2.5), is essential to the NS equations set. It describes the energy transfer within the fluid due to work, heat transfer, and energy dissipation.

$$\frac{\partial (\rho i)}{\partial t} + \operatorname{div}(\rho i \mathbf{u}) = -p \operatorname{div} \mathbf{u} + \operatorname{div}(K \operatorname{grad} T) + \Phi + S_i \tag{2.5}$$

where i is the internal energy, K is the thermal conductivity, T is temperature, Φ is the dissipation function, and S_i is the source term [26].

One of the main challenges with the NS equations is that they have to account for things happening simultaneously on different scales. Calculating all these different things simultaneously can be challenging, even for powerful computers. Furthermore, the NS equations are based on the assumption of laminar flow. However, in practical scenarios, flows frequently exhibit turbulence. Consequently, specialized methods and models are employed to account for this turbulence, aiming to predict the fluid behavior more accurately.

2.2.2 Turbulence Models

Turbulence is a common yet complex phenomenon that occurs when fluids such as water move in a chaotic, unpredictable manner. It plays a critical role in a variety of natural and technological events. Despite its significance, it remains one of the most challenging aspects of fluid dynamics to understand and predict accurately. Turbulence is hard to calculate because of the sheer complexity and randomness of turbulent flows, featuring a range of fluctuating scales, from large, swirling patterns to tiny, rapid fluctuations. To help with the study of turbulence, different methods and models have been developed to help simplify and approximate turbulent flows, making them easier to understand and predict. These models simplify turbulence's random, chaotic behavior into something more manageable. Some models average the fluid's motion over time, while others focus on the large patterns and ignore the smaller ones. A more detailed exploration of these strategies is presented in the following subsection.

Several methods account for the turbulence in a flow, each offering a different approach to simplify the problem. Direct Numerical Simulation (DNS) is a method that attempts to capture every detail of turbulence. It solves the NS equations across all turbulent scales without any approximations. While DNS yields highly precise flow predictions, its demand for extensive computational resources renders it less feasible for large problems, such as the lobe pump [26].

In contrast, the Large Eddy Simulations (LES) focus on resolving the NS equations in the large eddies and introduce approximations for the smaller, less nuanced details. This method, being less resource-intensive than DNS, compromises accuracy[26].

Another method is the Reynolds-Averaged Navier-Stokes (RANS), named after Osborne Reynolds. This method employs an averaged version of the NS equations to generalize the turbulence effects. RANS offers speed and reduced computational demands, positioning it as a practical solution for many problems. However, because it averages out the turbulence, RANS doesn't provide as detailed a picture of the flow as DNS or LES [26].

RANS is especially suitable for understanding fluid behavior within a lobe pump, primarily due to its efficiency and practicality. Lobe pumps create complex, three-dimensional fluid movements due to the rotational action of the lobes. These movements involve varying scales of turbulence and can be quite challenging to model accurately. However, because the RANS method averages out the effects of turbulence, it significantly simplifies these complex movements. This approach allows quicker computations and requires less computational power than DNS or LES. Furthermore, the detail RANS provides is sufficient for most practical design and operational considerations related to lobe pumps. Thus, RANS provides a suitable and resource-efficient method for modeling and understanding the fluid dynamics within lobe pumps.

Having established the practical advantages of the RANS method, it is appropriate to explore its foundational mechanics. Central to RANS is the principle known as Reynolds decomposition and its transition into the RANS equations, which offer a more tractable representation of turbulent flows. Reynolds decomposition breaks down the fluid velocity into two parts: a time-averaged part (mean flow) and a fluctuating part (turbulent fluctuations). These equations are then formed by taking the average of the original NS equations over a long period compared to the typical timescale of the turbulent fluctuations. The result is a set of equations similar to the original NS equations but with these extra terms representing the effects of turbulence. These are in Equation (2.6)-(2.9), representing the averaged continuity equation and the averaged momentum Reynolds equations, respectively. The additional terms represent a new problem, the closure problem, because there are more unknowns (Reynolds stresses) than there are equations. To "close" the system of equations, turbulence models, such as the $k-\epsilon$ or $k-\omega$ models, are used to express the Reynolds stresses in terms of known quantities. The effect of the turbulent fluctuations on the mean flow is accounted for through additional terms called Reynolds stresses [25].

$$\frac{\partial \rho}{\partial t} + \operatorname{div}(\rho \mathbf{U}) = 0 \tag{2.6}$$

$$\frac{\partial(\rho u)}{\partial t} + \text{div}(\rho u \mathbf{U}) = -\frac{\partial P}{\partial x} + \text{div}(\mu \,\text{grad}\, u) + \left[-\frac{\partial \overline{(\rho u'^2)}}{\partial x} - \frac{\partial \overline{(\rho u'v')}}{\partial y} - \frac{\partial \overline{(\rho u'w')}}{\partial z} \right] \tag{2.7}$$

$$\frac{\partial(\rho v)}{\partial t} + \text{div}(\rho v \mathbf{U}) = -\frac{\partial P}{\partial y} + \text{div}(\mu \,\text{grad}\, v) + \left[-\frac{\partial \overline{(\rho u'v')}}{\partial x} - \frac{\partial \overline{(\rho v'^2)}}{\partial y} - \frac{\partial \overline{(\rho v'w')}}{\partial z} \right] \tag{2.8}$$

$$\frac{\partial(\rho w)}{\partial t} + \text{div}(\rho w \mathbf{U}) = -\frac{\partial P}{\partial z} + \text{div}(\mu \,\text{grad}\, w) + \left[-\frac{\partial \overline{(\rho u'w')}}{\partial x} - \frac{\partial \overline{(\rho v'w')}}{\partial y} - \frac{\partial \overline{(\rho w'^2)}}{\partial z} \right] \tag{2.9}$$

where $\mathbf{U}$ is the mean velocity vector, P is the mean pressure, and the over-lined terms are the Reynolds stresses.

The Reynolds stresses are given in the term $\tau_{ij} = -\rho\overline{u_i' u_j'}$. These stresses reflect the influence of turbulent fluctuations on the mean flow and are crucial in treating turbulent flows. To simplify this complexity, the Boussinesq approximation is often employed. This approximation assumed that the Reynolds stresses behave similarly to the viscous stresses in a laminar flow, implying they are proportional to the mean deformation rate. This simplification allows the Reynolds stresses to be written as in Equation (2.10).

$$\tau_{ij} = -\rho\overline{u_i' u_j'} = \mu_t \left(\frac{\partial U_i}{\partial x_j} + \frac{\partial U_j}{\partial x_i} \right) - \frac{2}{3}\rho k \delta_{ij} \tag{2.10}$$

where μ_t is the eddy viscosity, $k = \frac{1}{2}(\overline{u'^2} + \overline{v'^2} + \overline{w'^2})$ is the turbulent kinetic energy per unit mass and δ_{ij} is the Kronecker Delta, which is equal to 1 if $i = j$ and equal to 0 if $i \neq j$ [26].

This formulation significantly reduces the complexity of the Reynolds stresses and is essential in providing a practical solution to the closure problem associated with the RANS equations. However, it's crucial to remember that the Boussinesq approximation is just that - an approximation based on the assumption of isotropic turbulence, which might not hold for all turbulent flows [26].

While the Boussinesq approximation is a significant step towards dealing with the turbulence issue, it introduces a new unknown into the equations: the eddy viscosity μ_t, also called the turbulent viscosity. It is important to note that turbulent viscosity is not a physical property of the fluid itself; rather, it is an abstract concept introduced to account for the effect of turbulence. This leads to the question - how can this turbulent viscosity be estimated?

Turbulence models provide a means to estimate the turbulent viscosity based on flow conditions and fluid properties. These models are key for applying the RANS equations to real-world turbulent flows. Some commonly used turbulence models are the $k-\epsilon$ model, the Wilcox $k-\omega$ model, and the SST $k-\omega$ model.

The $k-\epsilon$ model, a commonly used turbulence model, employs two variables: k represents turbulent kinetic energy, while ϵ designates its dissipation rate. While this model is useful for many situations, it does not very well handle the strong curvature and rapidly changing flow directions inside a lobe pump. This model's assumptions do not match the complex flow inside a lobe pump, so other models might give more accurate results [26].

The Wilcox $k-\omega$ model, another two-equation turbulence model, uses k to represent turbulent kinetic energy and ω for the specific dissipation rate. While it can handle certain flow complexities better than the $k-\epsilon$ model, it still faces limitations with complex geometries like a lobe pump. The flow inside a lobe pump can change rapidly and have strong curvatures, where the assumptions of the $k-\omega$ model may not hold, potentially leading to less accurate results [26].

The SST $k-\omega$ model

The Shear Stress Transport (SST) $k-\omega$ model is a turbulence model designed to capture the intricacies of real-world fluid flows more effectively. This model, a variant of the standard $k-\omega$ model, represents a significant breakthrough in handling turbulent flows in complex geometries. This model was suggested by Menter in 1992 [27].

At its core, the SST $k-\omega$ model is a fusion of the $k-\omega$ and $k-\epsilon$ models. It leverages the best aspects of both, providing a hybrid solution that outperforms each model under certain circumstances. Near the wall, where viscous effects dominate the physics of turbulence, it relies on the $k-\omega$ formulation, renowned for its accuracy and stability in boundary layers. Conversely, away from the wall and in the free-stream regions where the flow can be significantly affected by adverse pressure gradients, it transitions smoothly to a $k-\epsilon$ formulation. The $k-\epsilon$ model's robustness in handling adverse pressure gradients ensures a more accurate representation of the turbulent flow in these areas. The two models are blended smoothly using a blending function that considers the local flow characteristics [27]. This leads to a seamless transition between the two models, effectively providing the benefits of both models where they perform the best.

The transport equation for k is the same as for the Wilcox $k-\omega$ model, given as in Equation (2.11) [27].

$$\frac{\partial(\rho k)}{\partial t} + \operatorname{div}(\rho k \mathbf{U}) = \operatorname{div}\left[\left(\mu + \frac{\mu_t}{\sigma_k}\right) \operatorname{grad}(k)\right] + P_k - \beta^* \rho k \omega \tag{2.11}$$

where σ_k and β^* is constants, and P_k the turbulent kinetic energy production is given as [27]

$$P_k = \left(2\mu_t S_{ij} \cdot S_{ij} - \frac{2}{3}\rho k \frac{\partial U_i}{\partial x_j}\delta_{ij}\right)$$

The transport equation for ω is found from the transport equation for ϵ in the $k-\epsilon$ model by replacing $\epsilon = k\omega$. It is given as in Equation (2.12).

$$\frac{\partial(\rho\omega)}{\partial t} + \operatorname{div}(\rho\omega\mathbf{U}) = \left[\left(\mu + \frac{\mu_t}{\sigma_{\omega,1}}\right)\operatorname{grad}(\omega)\right] + \gamma_2\left(2\rho S_{ij} \cdot S_{ij} - \frac{2}{3}\rho\omega\frac{\partial U_i}{\partial x_j}\delta_{ij}\right) - \beta_2\rho\omega^2 + 2\frac{\rho}{\sigma_{\omega,2}\omega}\frac{\partial k}{\partial x_k}\frac{\partial \omega}{\partial x_k} \tag{2.12}$$

where S_{ij} is the rate of deformation, and $\sigma_{\omega,1}$, γ_2, $\sigma_{\omega,2}$, and β_2 is constants [27].

The Reynolds stresses are calculated using the Boussinesq approximation in Equation (2.10).

In 2003, Menter *et al.* proposed a series of modifications to the SST $k-\omega$ model, reflecting a decade's insight and experiences with the original model. A key part of these changes involved adjusting the constants within the model to $\sigma_k = 1.0$, $\sigma_{\omega,1} = 2.0$, $\sigma_{\omega,2} = 1.17$, $\gamma_2 = 0.44$, $\beta_2 = 0.083$, and $\beta^* = 0.09$ [28].

Furthermore, the blending functions were refined. The goal was to improve the predictions of turbulent behavior, particularly near the walls and in regions where the flow separates. The blending functions allowed a more gradual transition between the two constituent models comprising the SST $k-\omega$ model [28].

Limiters for the eddy viscosity and the turbulent kinetic energy production were also introduced. By imposing a limit in eddy viscosity, given in Equation (2.13), the model's performance could be enhanced for flows featuring adverse pressure gradients and in wake regions. The turbulent kinetic energy production limitation, given in Equation (2.14), was designed to prevent an excessive build-up of turbulence in stagnation regions [28].

$$\mu_t = \frac{a_1 \rho k}{\max(a_1 + \omega, SF_2)} \tag{2.13}$$

where $S = \sqrt{2S_{ij}S_{ij}}$, a_1 is a constant, and F_2 is a blending function.

$$P_k = \min\left(10\beta^*\rho k\omega, 2\mu_t S_{ij}\cdot S_{ij} - \frac{2}{3}\rho k\frac{\partial U_i}{\partial x_j}\delta_{ij}\right) \tag{2.14}$$

Boundary conditions for the SST $k-\omega$ model are defined similarly to those of the Wilcox $k-\omega$ model. At the inlet, k and ω values are specified, while a zero gradient is implemented at the outlet. The walls are assumed to be no-slip surfaces, and all turbulent quantities except ω are set to zero. Wilcox established a boundary condition for ω at y=0, as seen in Equation (2.15).

$$\omega = 10\frac{6\nu}{\beta_1(\Delta y)^2} \tag{2.15}$$

where ν is the kinematic viscosity and Δy is the distance to the next point from the wall [26].

These modifications bolster the model's accuracy and reliability in simulating complex turbulent flows in various practical scenarios.

In the context of lobe pump simulations, Ganz [23] have employed the SST $k-\omega$ model in the CFD solver methodologies, underscoring its suitability for such applications. A lobe pump comprises intricate geometries, and its operation induces complex flow phenomena such as flow separation, re-circulation zones, and adverse pressure gradients. These conditions present a considerable challenge to many standard turbulence models. However, the SST $k-\omega$ model, with its hybrid nature, is well-equipped to deal with these complexities.

The model's ability to accurately handle viscous effects near the wall regions ensures the intricate flow patterns associated with the rotating lobes are captured effectively. Simultaneously, its robustness in adverse pressure gradients allows it to accurately model the re-circulation zones and potential flow separations within the pump chamber.

Despite the SST $k-\omega$ model's robustness and superior performance in many flow scenarios, it is also computationally more demanding due to the additional blending function and shear stress transport formulation. However, the increased computational cost is often justified by the higher accuracy and reliability of the model, especially in complex flow scenarios such as those found within lobe pumps.

In conclusion, Menter's SST $k-\omega$ model offers a well-balanced approach for turbulence modeling, combining the strengths of the $k-\omega$ and $k-\epsilon$ models and effectively managing their limitations. Its ability to handle a variety of flow scenarios with high accuracy makes it a suitable choice for CFD simulations of lobe pumps.

2.2.3 Vortex Formation

A vortex is a region in a fluid where the flow is primarily a spinning motion about an imaginary axis. In lobe pumps, the intricate geometry and rotating motion of the lobes can induce vortex formation within the pumped fluid. Understanding the characteristics and dynamics of these vortices is important for optimizing pump performance and mitigating potential adverse effects on material, such as fish, in aquatic applications.

In a lobe pump, the lobes rotate to create low and high-pressure pockets as they mesh and un-mesh. When the lobes un-mesh, a low-pressure zone is created, pulling the fluid into the cavity. As the fluid fills this region, the velocity gradients along the walls of the lobes can lead to the formation of vortices. These vortices are more likely to form at higher rotational speeds and can be intensified by turbulent flow conditions.

There are two main types of vortices. The first one is leading-edge vortices. These form near the tips of the lobes as they begin to un-mesh and are characterized by a high velocity and lower

pressure region. The second type is trailing-edge vortices. These emerge at the tail ends of the lobes as they complete a rotation and are often smaller and less intense than leading-edge vortices.

Vortices could pose a risk in applications involving fish, such as for lobe pumps in seawater. High velocity and pressure gradients within vortices can cause shear stress, which may harm the fish. Therefore, understanding vortex dynamics is important for designing efficient and safe pumps for such specialized applications. Here, CFD offers valuable insights.

2.3 CFD

CFD uses numerical analysis and data structures to solve and analyze fluid flow problems. This section describes how CFD can provide a detailed understanding of fluid behaviors and interactions, particularly within complex structures such as lobe pumps in a low-head PHS system. CFD offers a comprehensive approach to studying fluid flow through numerical methods and algorithms. It allows for precisely simulating interactions between fluids and surfaces, represented by boundary conditions or as solids immersed within the fluid. CFD's inherent strength lies in its capacity to generate detailed and accurate results, thus accommodating complex geometrical configurations and diverse physical phenomena. The following section will explore the foundational principles of CFD, software, mesh generation, verification and validation, and the simulation setup for this study.

2.3.1 Principles of CFD

CFD is a powerful approach to analyzing and understanding fluid flow and heat transfer phenomena. By numerically solving the governing equations of fluid dynamics, CFD provides detailed insight into the intricate behaviors of fluid, also in systems with complex geometries, such as lobe pumps.

Before the CFD analysis, a fundamental step involves creating an accurate representation of the system's geometry, and this is where tools like SpaceClaim come into play. SpaceClaim, a CAD modeling software, provides a platform for engineers to design, edit, and prepare geometries for simulation. In the context of lobe pumps, the intricate contours, chambers, and rotors necessitate precision in design to ensure the simulations reflect real-world scenarios. It is also important to consider eliminating any unnecessary complexities or potential geometric errors, thereby creating a seamless transition from the design phase to the pre-processing phase of CFD.

The foundation of any CFD analysis begins with the pre-processing phase. The domain in which the fluid flow will be examined is defined during this stage. Any simplifications or assumptions necessary to make the simulation feasible are considered. The domain is then discretized into a mesh, or grid, of small elements. The mesh's quality and fineness directly influence the precision of the results. Boundary conditions, including velocity, pressure, and temperature, are meticulously outlined during this phase. To complete this section, properties of the fluid and any solid materials within the domain are specified, building upon well-established conservation laws and the NS equations [26].

After the pre-processing is the solver phase, where the primary task is discretizing the governing partial differential equations into a system of algebraic equations. Several methods facilitate this transformation, including the Finite Difference Method (FDM), which uses finite differences to approximate derivatives and is particularly effective for simpler geometries [29]. The Finite Volume Method (FVM), on the other hand, operates based on conservative law's integral form. FVM becomes a favored choice for simulations involving intricate geometries by ensuring local conservation [26]. Lastly, the Finite Element Method (FEM) stands apart, working to minimize an error function and offering unmatched flexibility when dealing with complex boundaries.

The IBM method is another technique that stands out for its ability to address complex boundaries by immersing them into a Cartesian grid, easing the computational challenges of unconventional

geometries. This method combines two solver methods: the finite difference method for solving flow patterns on a fixed grid and the finite element method to show how solid boundaries can move and interact with the fluid. Due to this combination, and because the finite difference method is used to solve the equations, IBM is seen as an explicit solver.

Once discretized, the system of algebraic equations is solved iteratively. The solution undergoes multiple refinements through iteration until convergence is achieved. For specific systems, such as lobe pumps with inherent turbulent flows, specialized turbulence models, like the SST $k-\omega$ model, are integrated into the solver, ensuring an accurate depiction of the flow behavior.

After the solver phase, the process ends with post-processing, focusing on interpreting and visualizing the results. Various tools come into play, visually representing parameters like velocity vectors, pressure contours, and temperature distributions. However, beyond these graphical insights, post-processing dives deep into quantitative analysis, revealing data points such as flow rates, drag coefficients, and heat transfer rates. A final yet crucial step involves validating and verifying the results to anchor the simulation's credibility and ensure its real-world relevance. This process underlines the authenticity and accuracy of the results and will be explained in Section 2.3.5.

2.3.2 CFD Software

While numerous CFD programs exist, a combination of SpaceClaim and Ansys CFX was chosen for this study. As a 3D CAD modeling platform, SpaceClaim offers flexibility in creating, editing, and refining geometries before analysis. Its user-friendly interface and intuitive design capabilities make it an invaluable tool for engineers aiming to achieve precise and optimal geometries for CFD simulations. For complex geometries like lobe pumps, this precision is essential.

Moreover, SpaceClaim's seamless integration with a broad spectrum of simulation tools, notably Ansys CFX, facilitates a smooth transition from design to simulation. With a simulation-ready model from SpaceClaim, one can effectively use the advanced features of CFD software to their fullest potential. Ansys CFX, building on this foundation, offers invaluable insight into fluid dynamics, also when studying the mechanisms of lobe pumps. Ansys CFX excels in its ability to handle turbulent flows, a common feature in lobe pumps. Tools like the SST $k-\omega$ model represent the intricate flow patterns, aiding a more comprehensive and accurate analysis. Another strength of CFX is the automatic meshing tool. The software efficiently breaks the complex geometry into smaller, manageable pieces. This ensures more accurate simulations, especially when there is movement in the components.

However, there are challenges. The depth of the features and options in CFX can be challenging, requiring a steep learning curve. Furthermore, the computational demands of the software are significant, meaning it necessitates robust hardware resources. CFX can provide detailed visualizations for lobe pump simulations - from flow trajectories to pressure variations. When used effectively, it is a tool that can enhance understanding and lead to informed decisions in both academic and professional settings.

Another challenge with Ansys CFX, as with most CFD software, is the potential to produce incorrect results if not properly used. Given the complexities of the fluid dynamics and different parameters, even a minor oversight of incorrect input can lead to significant errors in the results. This emphasizes the importance of a thorough verification and validation process. After running the simulations, ensuring that the results align with reality and theoretical predictions is essential. This will ensure the authenticity of the generated results.

In conclusion, despite the challenges inherent in Ansys CFX, its capabilities are commendable. When paired with SpaceClaim's design versatility, the duo emerges as an optimal choice for simulating flow within lobe pumps.

2.3.3 Mesh Generation

Meshing in CFD involves the subdivision of the computational domain into smaller, manageable elements, facilitating the solution of governing equations over the region of interest. These elements, often called cells, are the foundation for numerical techniques to approximate flow variables. Typically, meshes can be broadly categorized into two main types: structured and unstructured, as shown in Figure 2.3.

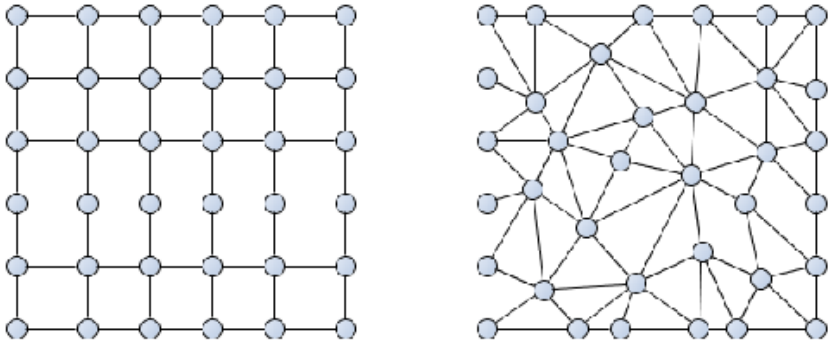

Figure 2.3: Structured mesh (left) vs. Unstructured mesh (right) [5]

A structured mesh comprises elements that follow a regular, predictable pattern, such as rectangles (in 2D) or hexahedra (in 3D). The consistent pattern ensures an ordered arrangement, which aids in simplifying the implementation of numerical methods. One significant advantage of structured meshes is their ability to offer high-quality cells, improving accuracy in areas with strong gradients, like boundary layers. However, generating a structure for complex geometries can be time-consuming and sometimes infeasible due to the inherent rigidity of its pattern.

On the other hand, an unstructured mesh employs elements that do not conform to a consistent pattern. Triangles (in 2D) or tetrahedra (in 3D) are typical shapes. Unstructured meshes provide great flexibility, making them well-suited for intricate geometries. This adaptability is their main advantage, as they can easily conform to irregular boundaries or fill complex spaces. However, they might require higher cell counts to achieve the same resolution as structured meshes, potentially increasing computational costs.

A structured or semi-structured hexahedral mesh is preferable for a lobe pump, considering the need for uniformity and precision in representing the pump's geometry. Hexa elements offer advantages in capturing the geometric intricacies of the lobe pump, which can be challenging for unstructured meshes to represent without significant refinement. The regularity of hexa meshes provides consistent and high-quality element shapes, which can lead to more accurate simulation results. The complex interplay of flow patterns within the pump, especially around the rotors, necessitates a denser mesh for capturing the transient dynamics effectively. Furthermore, regions near the tip gaps demand a refined mesh. This ensures that altered flow patterns are well-resolved.

When discussing mesh generation, the growth rate is an important factor. Essentially, this rate decides the relative size of mesh elements compared to the actual geometry. Industry standards are 1.2 for this value [30]. Choosing a value higher than this could risk the mesh's accuracy, mainly due to elements not aligning properly with the pump's curves. Conversely, a lower rate might provide a more refined mesh but at the expense of higher computational demands.

Inflation layers are another essential consideration in mesh generation, especially for flow simulations involving boundary layers. These thin layers of elements adjacent to walls or surfaces are designed to capture the flow variables' gradient more accurately near the walk. Inflation layers ensure a high resolution in regions with sharp variations in flow properties, such as velocity gradients near solid boundaries. Typically, these layers consist of the prism of hexahedral elements that gradually expand as they move away from the wall, allowing for a smoother transition to the core mesh. Incorporating inflation layers can significantly enhance the accuracy of the simu-

lation results, especially in predicting phenomena like boundary layer separation and wall shear stress. However, care must be taken to balance the number and thickness of these layers to ensure computational efficiency without compromising simulation accuracy.

The mesh's size and density, often called grid resolution, is another essential factor. While a high-resolution grid can accurately capture flow details and gradients, it requires more computational resources and time. Conversely, a low-resolution grid is computationally faster but may fail to capture flow features, resulting in a less accurate solution. Hand in hand with grid resolution is the concept of grid independence. It verifies whether the solution remains consistent irrespective of the mesh used. This concept will be further described in Section 2.3.5.

Mesh Metrics

Mesh metrics are quantitative measures used to ascertain the mesh quality. These measures - aspect ratio, orthogonal quality, and skewness - serve as a lens to examine element shapes and sizes within the mesh.

The aspect ratio examines the lengths of the sides of a mesh element. It is expressed as a ratio where the longest side is compared to the shortest side [31]. An aspect ratio of 1 suggests a perfectly shaped element. However, high values can signal distortions, which might misrepresent the physics in specific domain areas.

Moving to orthogonal quality, this focuses on how closely an element resembles a shape with perfect right angles. The more the angles of an element approach 90°, the better the orthogonal quality. If the orthogonal quality is 1, this indicates a perfect orthogonal element. A high-quality mesh ensures that the mesh surface is consistently smooth [31].

Lastly, there is skewness, which asses the symmetry of a mesh element. This is calculated by looking at how different the lengths of an element's sides are. Ideally, a low skewness value indicates elements that have almost equal side lengths, promoting a smoother overall mesh surface [31]. It is generally agreed that a skewness value should lie between 0 and 0.5. Utilizing these metrics helps ensure the mesh's quality, optimizing it for analyzing the pump and yielding precise outcomes.

2.3.4 2D vs. 3D Modeling in Lobe Pump Simulations

In computational simulations, selecting between a 2D or a 3D modeling approach, especially for intricate machinery like lobe pumps, is pivotal. The differentiation between these two modeling techniques is marked by their advantages and limitations, with the final choice often anchored in the study's goals, the resources at hand, and the system's intricacies under examination.

2D models stand out primarily due to their computational efficiency. Since they inherently demand fewer computational resources than 3D models, simulations can be executed more time-efficiently. This expedited process becomes invaluable during the early phases of a project, where swift iterations might be essential. This computational simplicity also translates to a more streamlined geometry, making the simulation setup and subsequent modifications relatively straightforward. For studies focusing on initial design or where the intention is to analyze overarching flow patterns without the intricacies of the third dimension, 2D models are particularly beneficial. Furthermore, from a cost perspective, the diminished computational needs of 2D simulations often translate to reduced expenses. Lastly, the visualization and interpretation of results from 2D simulations are usually more direct, devoid of the complications that the third dimension might introduce.

However, the merits of 2D modeling come with certain trade-offs. The most pronounced limitation is the reduced realism, given that real-world operations of lobe pumps are inherently three-dimensional. This might mean that 2D simulation might not encapsulate the full spectrum of physical processes within the pump. While sometimes advantageous, the inherent simplification that a 2D model offers can also lead to significant oversight in scenarios where the third dimension plays a crucial role. This limitation extends to being restricted to planar analysis, meaning

interactions outside this plane might be entirely missed. Moreover, any asymmetries in the geometry or flow conditions that would manifest distinctly in a 3D setting might be captured in a 2D framework, potentially skewing the understanding of the fluid dynamics in the pump.

The decision to employ a 2D or 3D model for lobe pump simulations is layered and multifaceted. While the simplicity and efficiency of 2D models have advantages, they might fall short in replicating the comprehensive interactions and behaviors typical of a lobe pump's operation. Conversely, 3D models, with their depth and detail, bring increased complexity and computational demands. Therefore, this decision should be made by weighing the project's objectives against the strengths and limitations of each approach.

2.3.5 Verification and validation

In computational studies, particularly when modeling real-world scenarios, there's an inherent need to ensure that the simulations are technically sound and genuinely reflective of reality. This is where the critical procedures of verification and validation come into play. However, a challenge in many computational simulations is the absence of real-world data for direct comparison. This is also the case for the simulation performed in this thesis. This lack can significantly complicate the validation process, and determining the accuracy and reliability of the simulation can become challenging. This situation demands other strategies and methods to confirm that the model is reliable, and this will be further explained in the following section.

Verification

Verification addresses the technical aspect of the model's implementation. It is used to ensure that the model is constructed correctly. This process examines whether the model, once implemented, matches the original design or concept. Issues related to software coding, algorithms, and numerical methods are explored to ascertain the model's integrity. Verification ensures no mistakes in how the model has been built.

Lobe pumps have a special design with two rotating parts that help move the fluid. This unique design means checking and rechecking the model for any mistakes. This is about ensuring the pump looks right and knowing it will work properly, especially in areas that might wear out or break over time. A model of a lobe pump needs to capture these details accurately.

The first step is to look at the software code when making a model for lobe pumps. This step ensures that there are no mistakes in the code and that everything runs smoothly. After that, the focus shifts to the calculation methods, like breaking a problem into smaller parts to make it easier to solve. It is crucial to select the right method, especially for showing how fluids move inside the lobe pump.

A key part of verification is changing some values in the model and seeing how it reacts. This means adjusting some details or settings and observing the results. This could mean changing the speed at which the pump parts move or the type of fluid used for lobe pumps. If the model's results change significantly with small adjustments, it might suggest a problem.

In CFD, the simulations need to stabilize, meaning reaching a consistent solution that does not change much with further calculations. To check this, the residuals are monitored during the simulations. The Root Mean Square (RMS) residuals can serve as a metric. Residuals represent the difference between the current simulation results and the previously computed set of results. When these differences, or errors, are small, it suggests that the model is settling down to a consistent solution. The RMS aspect of this metric involves squaring these differences, averaging them, and then taking the square root, which offers a solid measure of these inconsistencies.

These RMS residuals must reach a very low value for many CFD simulations to ensure accuracy. Typical convergence criteria are set to 10^{-4}. This ensures that the governing equations, representing physical phenomena such as momentum and energy conservation, are adequately resolved, leading to a trustworthy solution.

Another important aspect of the verification process is the grid independence study. The quality and size of the grid can influence the simulation results. A sensitivity analysis is typically conducted using different grid sizes to establish that the solution is grid-independent. Three different mesh levels are common:

- Coarse grid, which has a lower number of computational elements
- Medium grid, which strikes a balance between the coarse grid and fine grids in terms of the element count
- Fine grid, with the highest density of computational elements

By examining the results on these grids, one can identify the extent to which the solution is sensitive to grid refinement. A solution can be considered grid-independent when the variation in pivotal output parameters, such as pressure and velocity, between the medium and fine grids falls below a certain threshold. This threshold is often set to a tolerance of less than 5%.

Verification isn't a one-time thing. As the model updates or changes, it must be checked again. Every time there is a change, big or small, the model should be reviewed to ensure it is still accurate and trustworthy.

Validation

Validation focuses on the model's appropriateness in representing a real-world scenario. It seeks to find out if the model is right for the task. This step evaluates if the model's assumptions and input parameters align with real-world conditions and behaviors. It is about ensuring the model's foundation aligns with actual observable phenomena. However, the task becomes notably challenging when there is a lack of full-scale experimental data for reference.

One potential solution to this challenge is to turn to experimental data from similar or scaled-down versions of the equipment in question, such as a pump. Even if not an exact representation, such data can offer valuable insights. By comparing the model to these data sets, it is possible to gauge its capacity to depict primary flow phenomena. However, it is crucial to tread carefully when generalizing these findings to the full-scale scenario, as certain phenomena might not exhibit linear solubility.

In scenarios where even scaled-down experimental data are unavailable, an option exists to align the model with theoretical expectations and benchmark against results from analogous studies or applications. While not a direct validation route, this strategy is a comparative measure to evaluate if the model's outcomes resonate with the established knowledge within the discipline.

Communicating transparently regarding the model's limitations and uncertainties in the simulation outcomes remains important. Such clarity ensures that those relying on the model are equipped to discern its relevance and reliability concerning their specific requirements.

Both validation and verification are foundational to any computational model's credibility. Ensuring a model's technical correctness and real-world relevance is important for its results to be useful.

2.4 Simulation Setup

Understanding the fluid movement in a lobe pump requires a careful simulation setup. This section will cover three main aspects of the specific simulation setup for this thesis. First, the pump's geometry will be described, which is what the simulation will be based on. Next, the meshing of the pump will be explained, and finally, the numerical setup will be described.

2.4.1 Geometry

The lobe pump geometry selected for this thesis aligns with the one used in the ALPHEUS project: a three-lobe pump featuring epicycloidal and straight lobes. Notably, a 2D design was adopted for this thesis, primarily due to the project's time constraint and because a 2D framework often simplifies problem-solving and accelerates computation without sacrificing key insights. Ansys CFX does not allow for the creation of purely 2D models. To overcome this and ensure compatibility, the model was made with a 3 mm thickness in the z-direction to create a pseudo-3D model.

The geometry introduced in this study draws inspiration from a 2D representation of the stator geometry presented by Gans. To enhance this foundational structure, epicycloidal lobes, sourced from the work of Valery Chernoray at Chalmers University for the ALPHEUS project, were incorporated, shown in Figure 2.4. Following the placement of these lobes within the stator framework, an encompassing casing was designed. The entire design process was adeptly managed using SpaceClaim, and the complete geometry with measurements is shown in Figure 2.5.

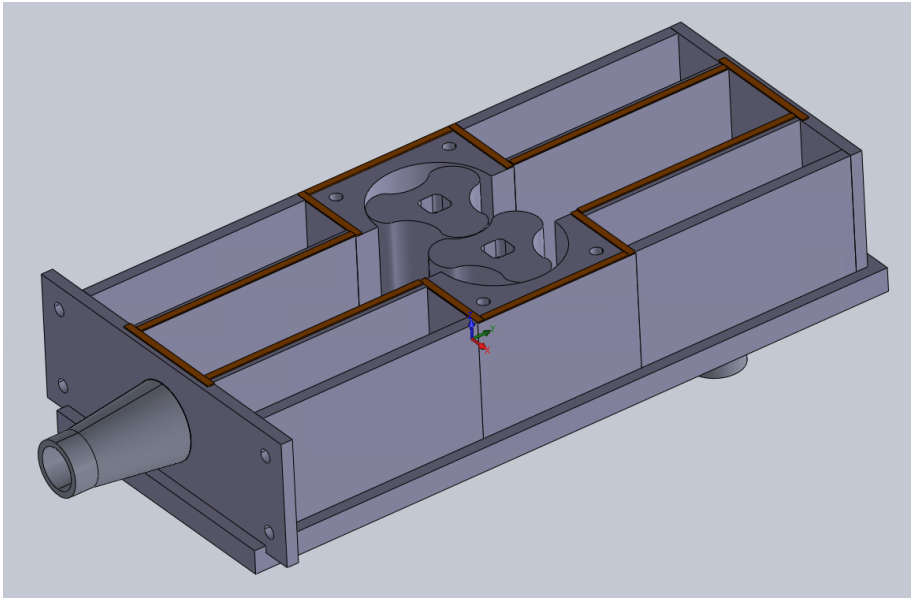

Figure 2.4: Complete setup of the CAD design by Chernoray. The illustration encompasses the epicycloidal lobe design used

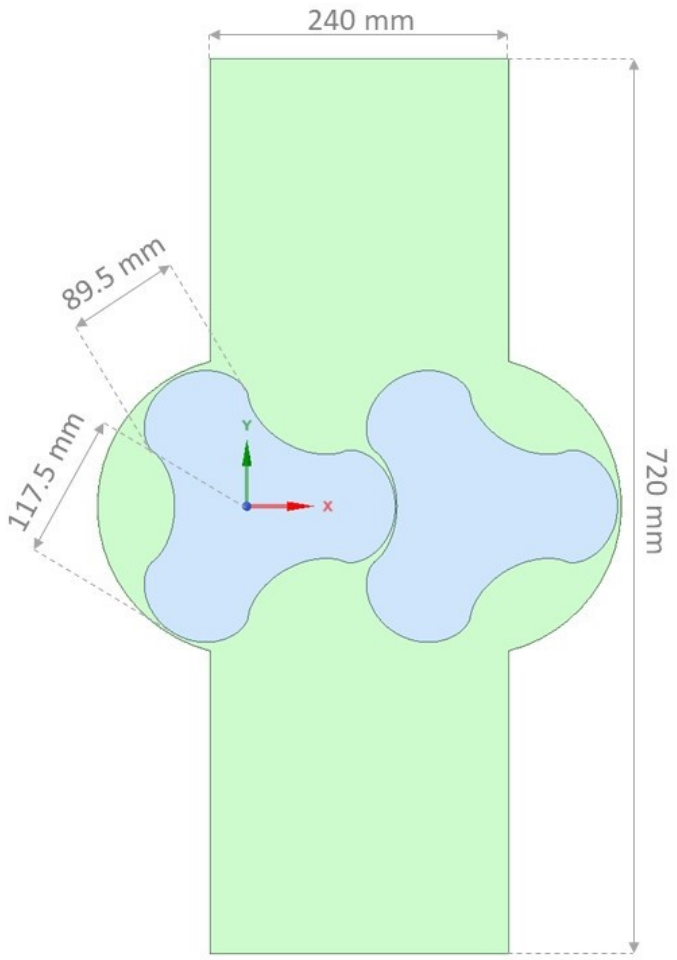

Figure 2.5: Complete lobe pump design with measurements

The clearance gap in the present geometry has been set to be 1 mm. In contrast, the geometry employed by Gans [23] adopted a clearance gap of 0.5 mm for all gaps between the casing and the lobes. Given the augmented dimensions of the pump in this thesis, a 1 mm clearance gap was deemed appropriate to maintain a proportional geometric consistency. While this choice aims for optimal performance, it is acknowledged that future refinements may necessitate adjustments to this specification. However, the scope of the current study does not prioritize this aspect.

Following, Named Selections were formulated in SpaceClaim, streamlining the task of defining boundary and initial conditions for the simulations. Before transitioning to Ansys Meshing, the geometry underwent thorough checks in SpaceClaim to ensure its integrity, confirming the absence of errors such as incomplete curves. This stage ensures a smooth and accurate importation of the design into Ansys Meshing and later into Ansys Pre.

2.4.2 Mesh Generation

The meshing quality significantly influences the simulation accuracy in CFD. An appropriate mesh ensures that the computational model captures the intricate physical phenomena, particularly in complex systems like a lobe pump.

The element size forms the basis of any meshing strategy. This study selected an element size of 1.5 mm after considering various factors. A finer mesh might offer more detail but at the cost of computational efficiency. Conversely, a coarser mesh, while faster, might not capture the subtle flow patterns, especially those that might impact aquatic life like fish. A grid independence study

was initiated to ascertain if this choice was suitable. The element size for the coarser grid was chosen to be 1.5 times larger, i.e., 2.25 mm, and an element size 1.5 smaller for the finer grid, i.e., 1 mm. The chosen size of 1.5 mm aims to strike a delicate balance, capturing the pump's geometry and the flow intricacies without significantly burdening computational resources.

As mentioned in the previous subsection, a depth of 3 mm in z-direction was introduced to create a pseudo-3D mesh. The chosen element size gives two elements in the z-direction, shown in Figure 2.6. This is primarily to maintain numerical stability. A single cell in the z-direction can lead to instabilities during the computational process. At least two cells will ensure a more robust numerical outcome. Additionally, turbulence models, such as the SST $k-\omega$, demand a uniform resolution across all dimensions. A single cell layer in the z-direction might undermine the accuracy of turbulence effects.

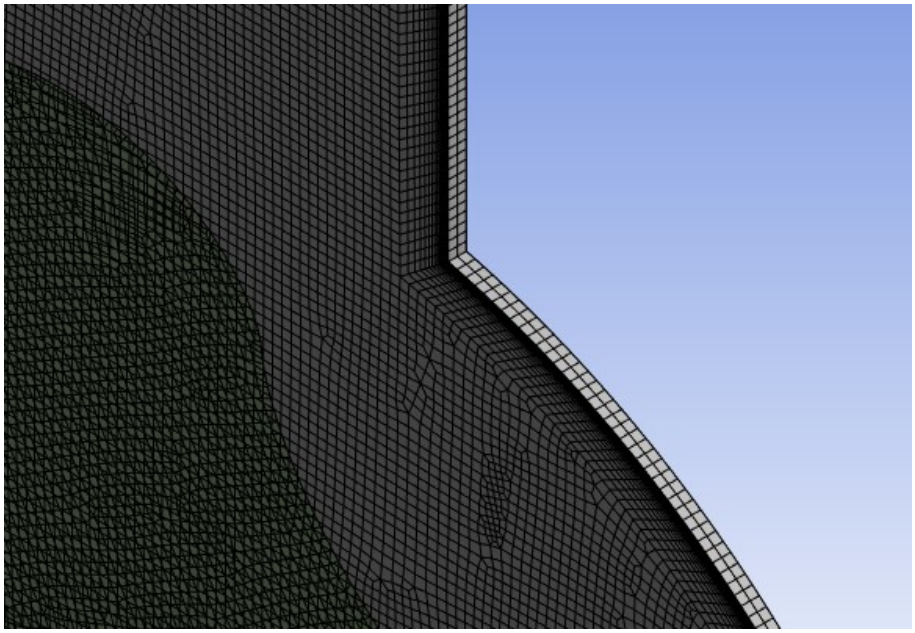

Figure 2.6: Mesh with two elements in the z-direction

One of the key regions in any fluid flow simulation is the boundary or the wall region. Here, fluid behavior changes drastically, often influencing the overall flow patterns. 30 inflation layers were incorporated into the mesh next to the wall, with a growth rate of 1.2. Their thickness was restricted to a maximum of 10 mm to prevent these layers from dominating the mesh. These measures ensure that near-wall phenomena are captured, which is crucial for understanding the effect on aquatic life. The inflation layers at one of the stator walls are shown in Figure 2.7

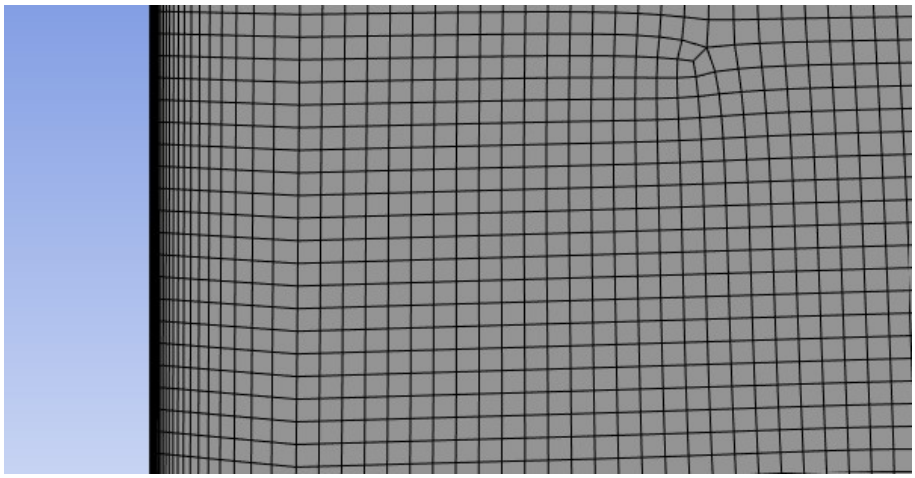

Figure 2.7: The inflation layers along the stator wall

The clearance gaps - between the lobes and the casing and between the lobes themselves - present a particularly challenging yet important area to simulate accurately. These narrow spaces often create intricate flow patterns and pressure variations that drastically affect pump performance and flow patterns. The element size of 1.5 mm, combined with the inflation layers at the boundaries, was also chosen to address these challenges. The mesh in the clearance gap between the left lobe and the casing is shown in Figure 2.8.

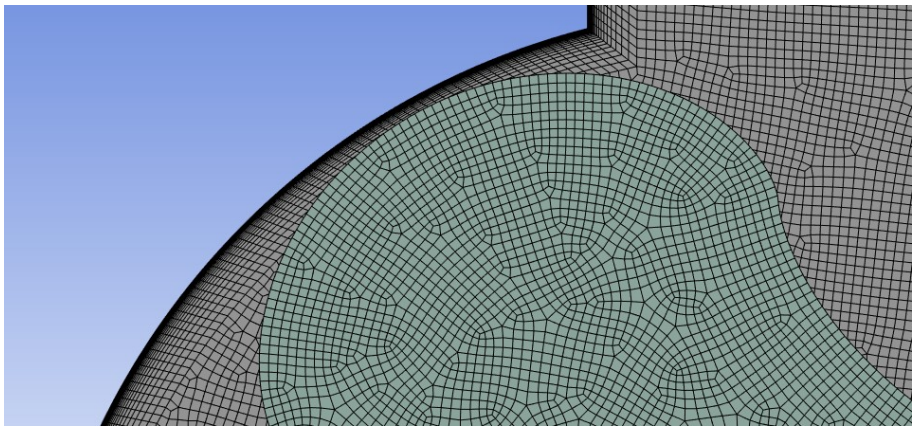

Figure 2.8: Mesh in the clearance gap between the left lobe and the casing

The MultiZone meshing method, known for its suitability for complex geometries, was chosen for the lobe pump model. Using hexahedral (or hexa) elements, this method offers a structured and organized mesh alignment. The structured mesh is suited for tracing flow patterns, which is particularly important given the study's focus on aquatic life. Figure 2.9 shows the lobes and casing mesh.

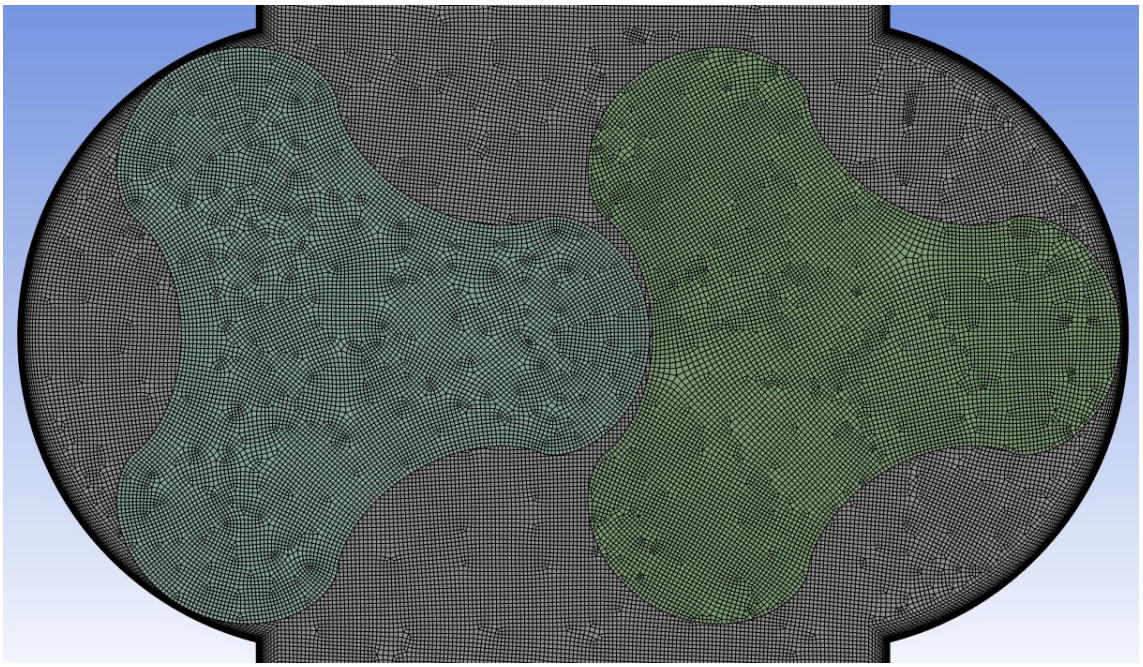

Figure 2.9: Mesh of lobes and casing

When generating the mesh, ensuring its quality is important. A well-constructed mesh can provide insight into subtle flow patterns, eddies, and vortex formations, which might pose a risk to aquatic life when subjected to the pump's operations. Hence, post mesh-generation, the mesh metrics were controlled, ensuring the reliability of the simulations.

2.4.3 Numerical Setup

The lobe pump simulations were established using two default domains corresponding to each lobe. These domains, classified as immersed solids, were set to rotate with speeds from 30 to 60 RPM, in line with the parameters of the ALPHEUS project. However, the study also explores higher speeds, reaching up to 500 RPM. The reason for including these higher RPM values is to examine the flow conditions under these more extreme conditions, which can be used to predict the impact on fish. One lobe exhibits positive rotation, while the other follows a negative direction. The specific rotation start and end points for the lobes were also defined.

To closely represent the real-world operation of the pump, boundary conditions were implemented. As identified through Named Selections, the inlet operates under a subsonic flow regime and maintains a static pressure of 1 atm, equivalent to 101 325 Pa. This ensures a stable and consistent flow at the simulation's entry point. Both the inlet and outlet are characterized as openings. The outlet serves as an exit path for the fluid post-engagement with the pump mechanism. The outlet's flow remains subsonic, but the static pressure is adjusted according to the head, which varies from 2 m to 12 m.

For this study, a head of 12 m was specifically chosen for all simulations. This head corresponds to an outlet pressure of 219 045 Pa. It can be assumed that this value has the potential to cause most distress to fish due to elevated pressure levels from inlet to outlet. The outlet pressure is calculated as in Equation (2.16).

$$P_{outlet} = 1\text{atm} + \rho \cdot g \cdot H \tag{2.16}$$

where P_{outlet} is the outlet pressure, g is the gravitational constant, and H is the water head.

The main conduit for the fluid, named the Default Domain, is allocated for water. No heat

transfer was considered within this domain, allowing the simulation to concentrate solely on the fluid dynamics. The turbulence model selected was the SST $k-\omega$ model. Uniform initial conditions were applied with a velocity set to 0 m/s in all three directions: x, y, and z. All boundaries were defined as no-slip walls.

A transient analysis was selected for the simulation to capture the fluid's time-dependent behaviors. Selecting an appropriate time step and simulation length is essential for accurately capturing complex flow phenomena, such as vortices and turbulent flow. One significant factor when determining these parameters is the rotational speed of the lobes. A faster rotational speed results in quicker changes in flow patterns, requiring a smaller time step to capture these rapid variations effectively. For example, at 500 RPM, a much smaller time step is needed compared to a speed of 30 RPM to ensure numerical stability and precision. The rotational speed also influences the simulation length. This study chooses the simulation length to cover multiple full rotations of the lobes. The different lengths and time steps for the different rotational speeds are presented in Table 2.1.

Rotational Speed	**Simulation Length**	**Time Step**
30 RPM	20 s	0.02 s
60 RPM	10 s	0.01 s
100 RPM	6 s	0.006 s
200 RPM	3 s	0.003 s
300 RPM	2 s	0.002 s
500 RPM	1.2 s	0.0012 s

Table 2.1: Length and time step for different rotational speeds

For post-processing and subsequent analyses, certain parameters were prioritized. Transient results for pressure and velocity were recorded to chronicle the fluid's dynamic shifts as it navigated through the pump. Additionally, the velocity in the Stationary Frame was documented, providing insight into the fluid's movement concerning the lobes. This data was collected at every time step, presenting a high-resolution dataset essential for the post-simulation analysis.

Regarding convergence criteria, a threshold of 10^{-4} was set for the RMS residuals. Establishing clear criteria for these residuals helps to achieve a more trustworthy solution.

Chapter 3

Results and Discussion

This chapter presents the detailed results and discussion of the study of lobe pump operations and interactions with fish. The chapter is divided into two main parts: results and discussion. The results section starts with a review of the mesh metrics, providing insight into the computational mesh used for the simulations. Next, the grid independence study is presented, ensuring the findings remain consistent across different mesh sizes. The core simulation results will be presented, shedding light on the fluid behavior within the lobe pump at various rotational speeds.

In the discussion section, the results will be verified and validated. The overall function of the pump will be analyzed first, followed by a closer look at its potential effects on marine life, especially fish - the main objective of this study. The chapter addresses the results' relevance and points out this study's limitations.

Overall, this chapter presents a blend of specific results and different perspectives, all angled toward the main objective of this thesis: understanding the impact of lobe pump operations on the surrounding marine life.

3.1 Mesh Metrics

The quality of the mesh was evaluated based on three different mesh metrics. The results are presented in Table 3.1. Each mesh metric provides distinct insight into the overall quality of the mesh and its potential implications on the simulation accuracy and reliability.

Element Size [mm]	**Mesh metric**	**Min.**	**Max.**	**Avg.**
1.5	Aspect Ratio	1.0002	232.2900	10.4650
	Orthogonal Quality	0.6560	1.0000	0.9777
	Skewness	1.2400e-4	0.6104	0.0820e-2

Table 3.1: Mesh metrics for the mesh of element size 1.5 mm

Concerning the aspect ratio, the mesh has a minimum value of 1.0002, indicating that a substantial part of the mesh elements are nearly optimally shaped. However, the maximum aspect ratio is 232.2900, signifying that certain regions within the mesh may contain considerably elongated elements. Although somewhat elevated, the average aspect ratio of 10.4650 remains within a range deemed acceptable for many engineering applications.

The orthogonal quality metrics further illuminate the mesh's quality. The mesh has a commendable minimum orthogonal quality of 0.6560, and the watch that the maximum orthogonal quality reaches up to 1.0000 signifies the mesh's consistency and adherence to high-quality standards. The overall average value of 0.9777 underscores this consistency across the entirety of the mesh.

Skewness values present additional insight. The mesh maintains a low minimum skewness of

1.2400e-4. While the maximum skewness is 0.6104, it remains within acceptable boundaries, suggesting that the overall mesh quality has not been compromised. The average skewness further affirms this, with a value of 0.0820e-2, emphasizing that the mesh is well within the desired standards.

In summation, the mesh metrics convey high reliability and quality. Though the aspect ratio raises minor concerns due to potential elongated regions, the orthogonal quality and skewness instill confidence in the mesh's suitability for precise simulations.

3.2 Grid Independence Study

An important step to ensure the reliability of any CFD study is conducting a grid independence study. This analysis is important as it ensures that the mesh's element size does not excessively influence the simulation results.

For this grid independence study, the rotational speed of 100 RPM was selected, given its significance in the overall pump analysis. Three mesh sizes were evaluated and compared: 1 mm, 1.5 mm, and 2 mm. The primary objective was to ascertain if the results varied substantially with changes in mesh size or if they exhibited a convergence trend, indicating grid independence.

Residuals for each mesh size were monitored to ensure the stability of each simulation. A comparison of the maximum velocity at a given timestep was performed. As a primary result parameter, the velocity should be consistent across different mesh sizes if the grid is truly independent. It was deemed acceptable if the maximum velocities between the meshes were within a 5% difference. Table (3.2) presents the maximum velocities observed for three distinct mesh element sizes: 1 mm, 1.5 mm, and 2 mm. The differences in maximum velocities between the element sizes are also provided.

Element Size [mm]	**Max. Velocity [m/s]**	**Difference [%]**
1.0	6.74	3.59
1.5	6.57	-
2.0	6.39	2.78

Table 3.2: Maximum velocities and difference for the different element sizes

When comparing the 1 mm mesh to the 1.5 mm reference mesh, the maximum velocity differs by approximately 3.59%. Similarly, the 2 mm mesh shows a velocity difference of about 2.78% relative to the 1.5 mm mesh. Both differences are within the permissible limit of 5%, suggesting that the chosen mesh resolution, especially the 1.5 mm mesh, offers an acceptable trade-off between computational efficiency and solution accuracy. This reinforces the confidence in the results and indicates that the mesh sizes chosen can capture the essential flow characteristics without introducing significant numerical errors.

For all tested mesh sizes, the RMS residuals were monitored to assess the convergence behavior and stability of the simulations. Across the board, the residuals demonstrated consistent and stable patterns, confirming that the simulations achieved a reliable solution regardless of the mesh size. Such consistent behavior of the residuals lends additional credibility to the results, reinforcing the assertion that the simulations are both robust and dependable across the various grid resolutions.

The grid independence study underscores the importance of selecting an appropriate mesh size for reliable simulations. Consistent results across various mesh sizes enhance confidence in the study's findings. The minimal differences observed indicate that the outcomes are not only dictated by mesh density but are genuine representations of the fluid dynamics within the pump. Thus, choosing a 1.5 mm mesh size offers an effective balance between computational demands and accurate data representation.

3.3 Simulation Results

This section presents simulation results for the lobe pump, operated at various rotational speeds, including 30 RPM, 60 RPM, 100 RPM, 200 RPM, 300 RPM, and 500 RPM. The simulations focus on key fluid dynamic characteristics such as velocity profiles, streamline patterns, and pressure distributions. Further, the accuracy and reliability of these simulations are verified by examining the residuals.

It should be noted that all figures presented in the following section are taken from points in the simulation where lobes have completed enough rotations to achieve a repeating pattern. Additionally, the snapshots are selected at moments when the lobes are in approximately the same positions. These two factors enable more accurate comparisons between different rotational speeds.

3.3.1 Velocity Profiles and Streamlines

This results subsection explores velocity profiles and velocity streamlines at rotational speeds ranging from 30 to 500 RPM, presented in Figure 3.1 to 3.6. The velocity profiles offer insight into the fluid flow characteristics, while the streamlines provide a comprehensive view of fluid movement patterns inside the pump. Together, they contribute to a more complete understanding of the fluid dynamics that fish might encounter when passing through the pump.

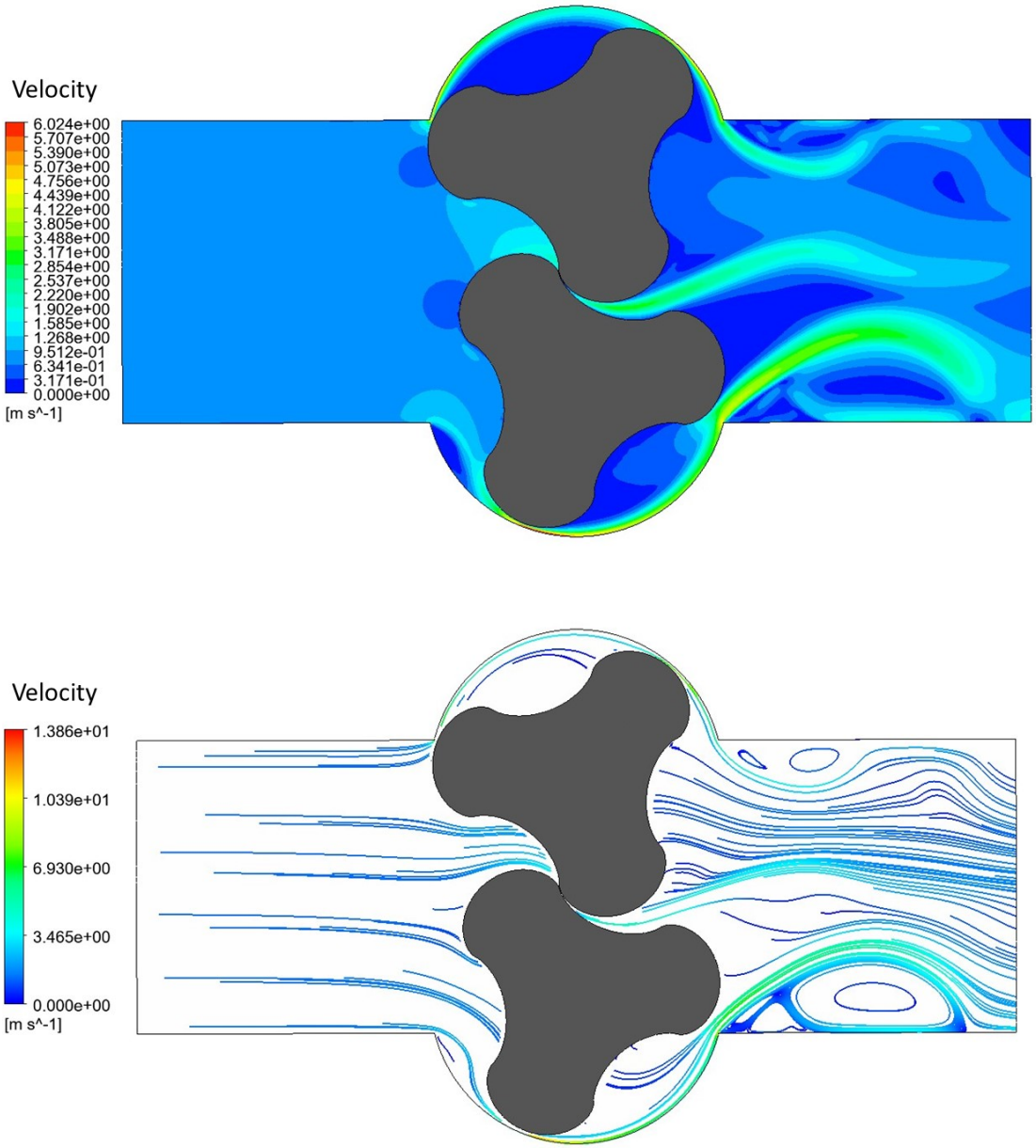

Figure 3.1: Contour of velocity profile and velocity streamlines for 30 RPM

The visuals for 30 RPM, presented in the figure above, serve as an important baseline for the study. The velocity profiles and streamlines exhibit relatively smooth transitions, indicative of a less chaotic flow field at this rotational speed. The circular features near the walls in the outlet section of the pump are noteworthy, which likely emerge from the combination of boundary layer effects due to the no-slip walls, and the heightened velocity as the fluid exits the lobes. While these patterns are subtle at 30 RPM and don't dictate the overall flow dynamics, they are important markers that help contrast the fluid behavior as the rotational speed increases.

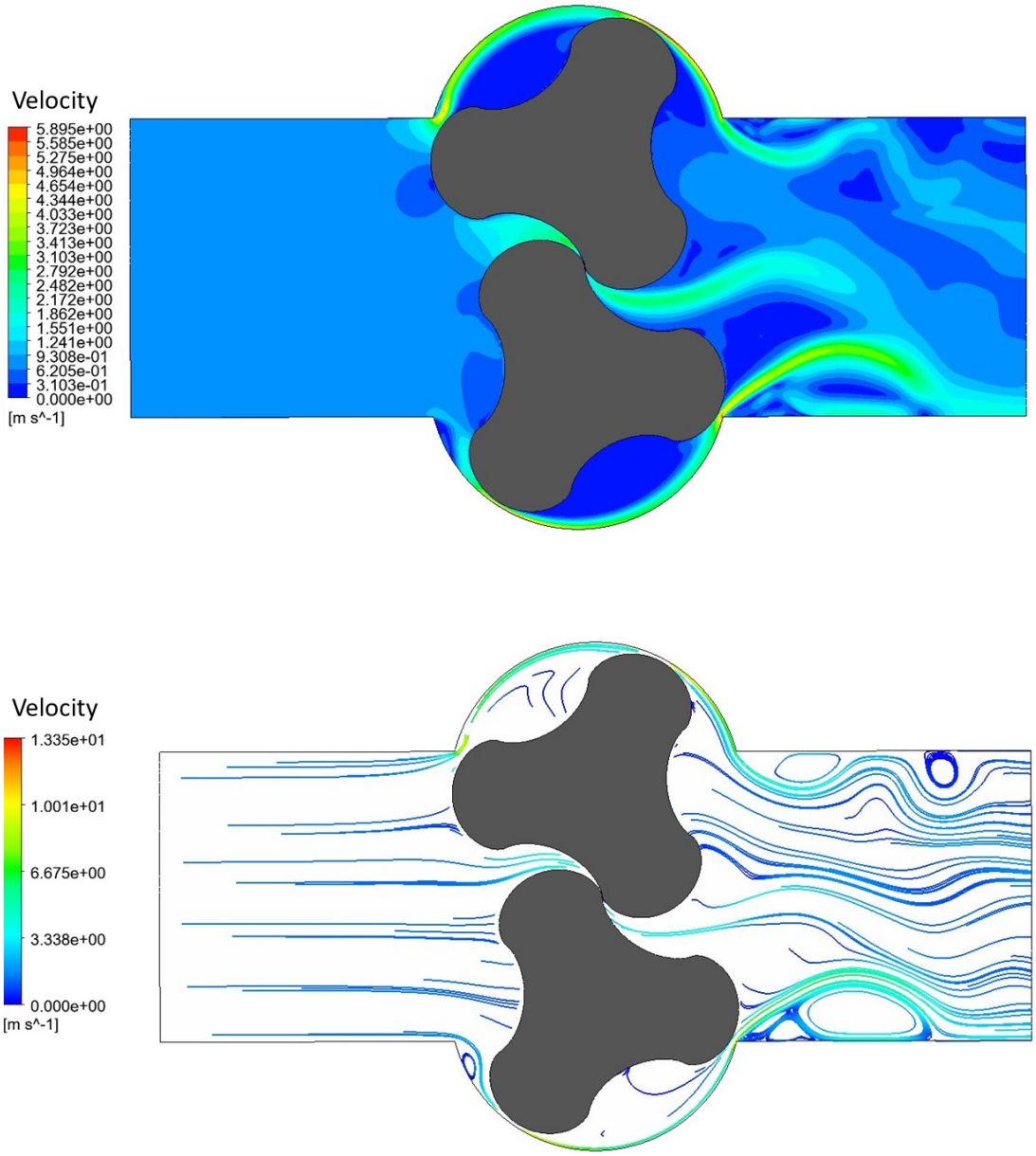

Figure 3.2: Contour of velocity profile and velocity streamlines for 60 RPM

For 60 RPM, the streamlines show a slight increase in complexity, featuring more noticeable fluctuations compared to the smoother flow at 30 RPM. Despite the added intricacies in the flow pattern, the velocity magnitudes remain similar to those observed at 30 RPM. These nuanced changes in the flow field suggest that although the rotational speed has increased, it hasn't significantly altered the overall velocity profile.

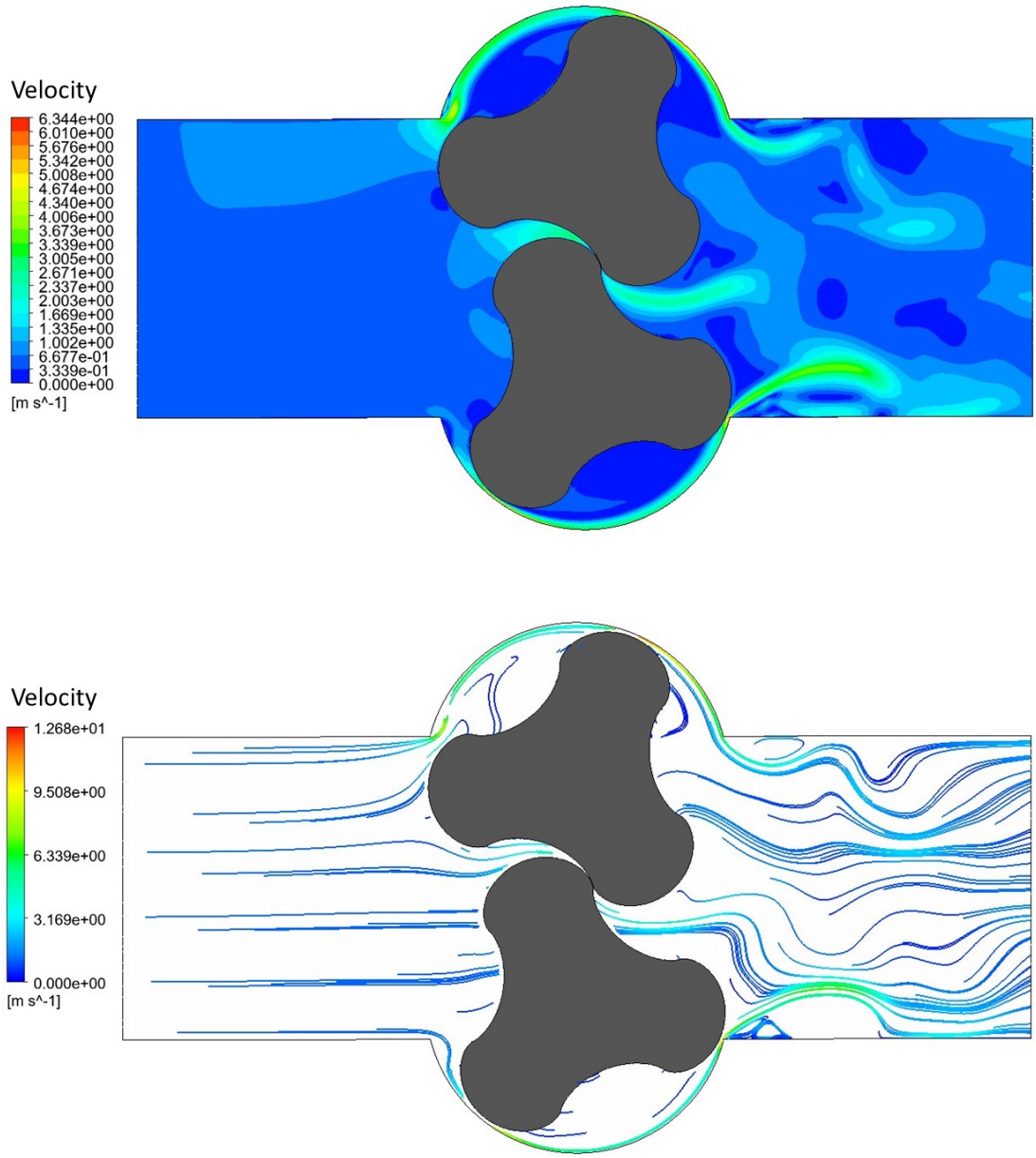

Figure 3.3: Contour of velocity profile and velocity streamlines for 100 RPM

At 100 RPM, the simulations reveal more fluctuating streamlines and velocities, particularly at the outlet side of the pump. This suggests a higher level of mixing as the flow moves through the system, compared to the flow at 30 and 60 RPM. This heightened mixing could even out the velocity variations across the flow field. As a result, the outlet velocities at 100 RPM remain in the same range as those at 60 RPM, which could result from increased fluid mixing inside the pump.

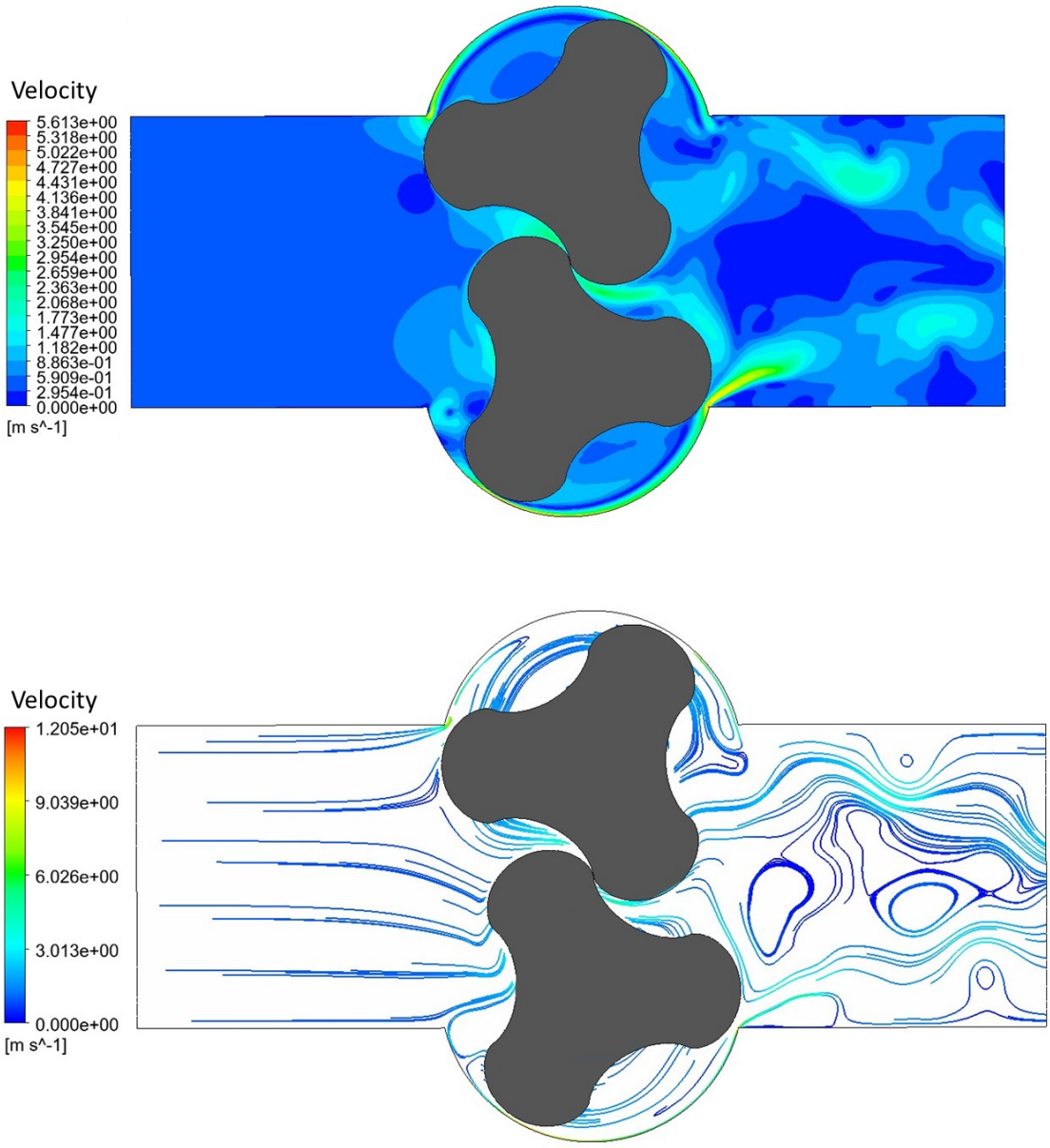

Figure 3.4: Contour of velocity profile and velocity streamlines for 200 RPM

At 200 RPM, the flow characteristics within the pump advance further. Increased mixing and intricate flow patterns surpass those seen at 100 RPM. The pronounced circular formations at the outlet side might be early signs of vortex activity, which can be a precursor to turbulence. These formations likely enhance the flow's complexity and mixing. Velocities upon exiting the lobes are observably higher than at 100 RPM, signifying the fluid's enhanced energy due to the escalated rotational speed.

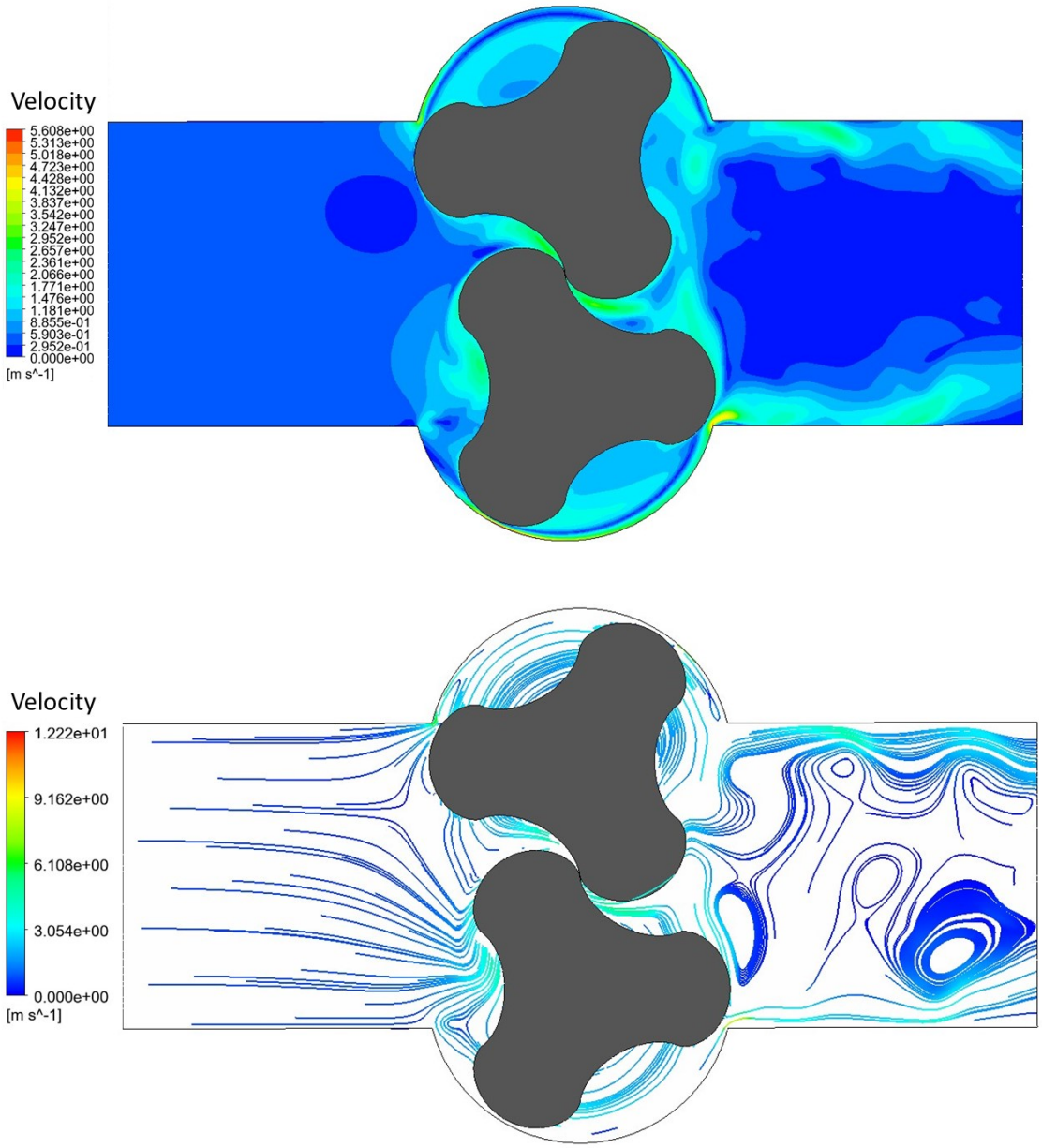

Figure 3.5: Contour of velocity profile and velocity streamlines for 300 RPM

For the rotational speed of 300 RPM, several distinct flow characteristics emerge. At the outlet side, the most elevated velocities are found nearer the walls, differing from the prior observations at lower RPMs. This might indicate an initial transition to turbulence, especially along the wall-bound flow. Central regions of the pump's outlet side exhibit noticeable circular motions and potential early-stage vortex formations hinting at more turbulent interactions. Furthermore, when considering the fluid's movement within the pump itself, a heightened velocity is observed compared to earlier cases, reflecting the influence of the increased rotational speed on the flow dynamics.

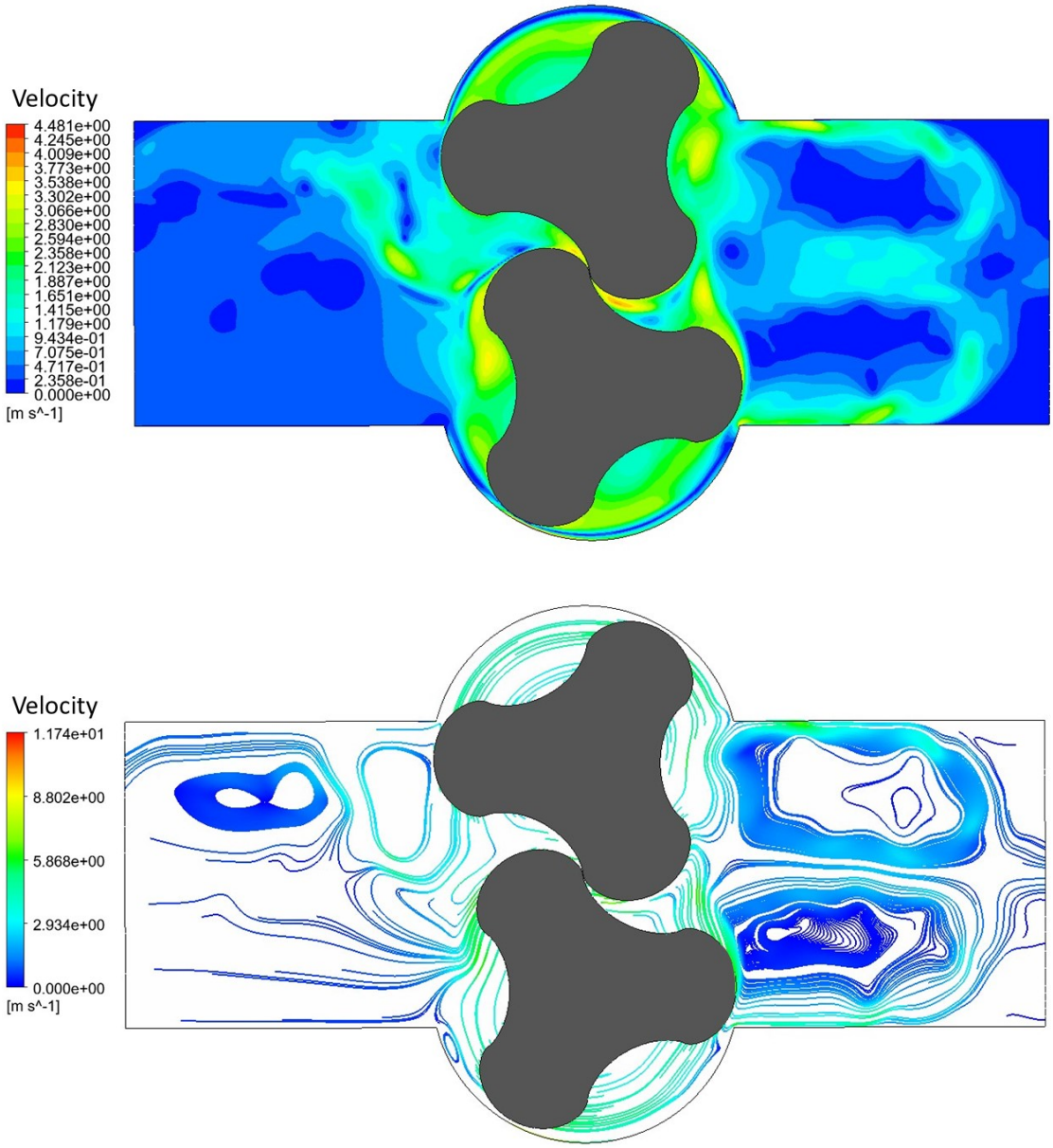

Figure 3.6: Contour of velocity profile and velocity streamlines for 500 RPM

At the pronounced 500 RPM, the pump's internal flow exhibits significant alterations. Streamlines predominantly form circular patterns, evident at both the inlet and especially dominant at the outlet. These swirling patterns likely represent mature vortex behaviors, indicating turbulence within the flow. Internally, the fluid's speed accelerates considerably, maintaining this velocity as it progresses past the lobe sections. When viewed alongside the velocity profile, this enhanced velocity shows a substantial part of the fluid's energy feeding into the circular patterns, suggesting the dominant influence of turbulence. Such pronounced vortex activity contrasts the simpler, more linear flow at lesser RPMs.

In summary, the velocity profiles and streamlines offer valuable insights into the fluid dynamics within the lobe pump at various rotational speeds. These visualizations are essential indicators for evaluating the pump's operational efficiency and its possible influence on marine life. With this foundational understanding of the flow characteristics, the following section will examine another critical aspect of fluid dynamics: pressure distributions within the lobe pump.

3.3.2 Pressure Distributions

Changes in pressure are key parameters that could influence the well-being of the fish in transit through the pump. The distribution of pressure at different rotational speeds aims to identify potential conditions that may harm marine life. The pressure distributions are presented in Figure 3.7 to 3.12 for a rotational speed of 30 to 500 RPM.

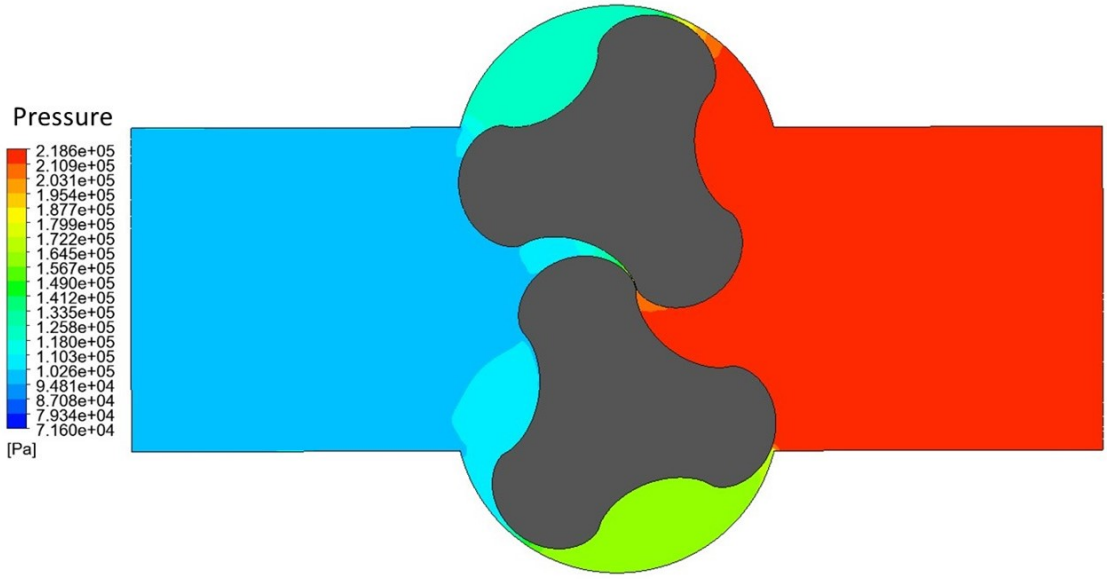

Figure 3.7: Contour of pressure profile for 30 RPM

The pressure distribution at 30 RPM exhibits distinct characteristics that align with the simulation's set inlet and outlet pressures. Specifically, the pressure at the inlet side of the pump is largely consistent with the preset inlet pressure, though there is a slight increase close to the lobes. A notable characteristic is the elevated pressure in the space between the lobes and the casing, which is higher than the inlet pressure but lower than the outlet pressure. The pressure levels off to match the preset outlet conditions on the outlet side of the lobes. The limited fluctuations in pressure could indicate minimal mixing within the fluid flow at this low rotational speed. This characteristic aligns well with the minimal mixing in the velocity profile at 30 RPM.

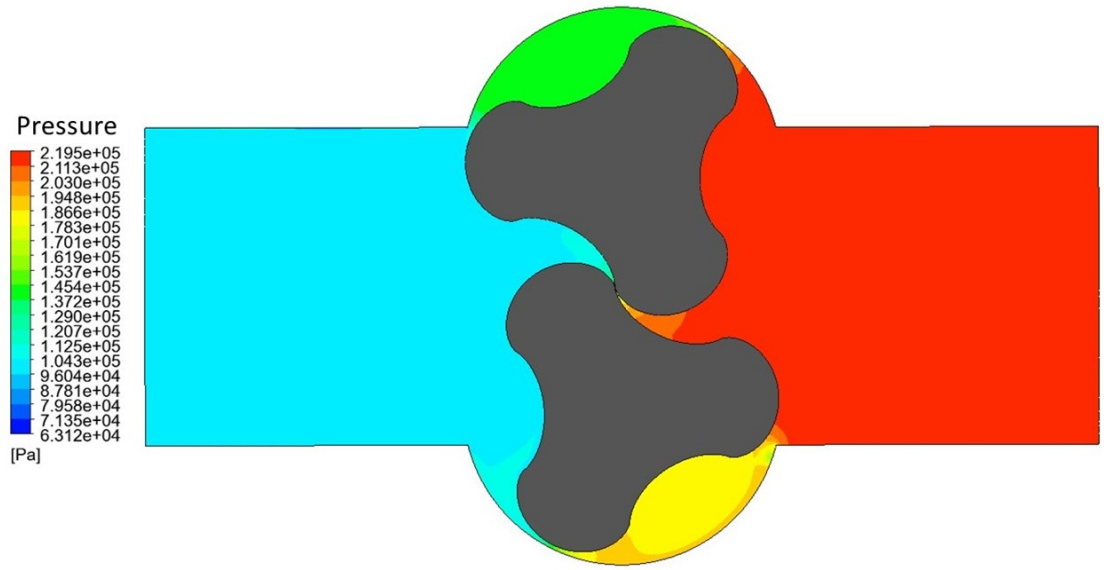

Figure 3.8: Contour of pressure profile for 60 RPM

For 60 RPM, the pressure distribution largely mirrors that observed at 30 RPM, with one notable distinction: an increase in pressure is observed in the space between the lobes and the casing. This elevated pressure suggests enhanced fluid interaction at this higher rotational speed, although the general pressure characteristics remain mainly consistent with the 30 RPM scenario.

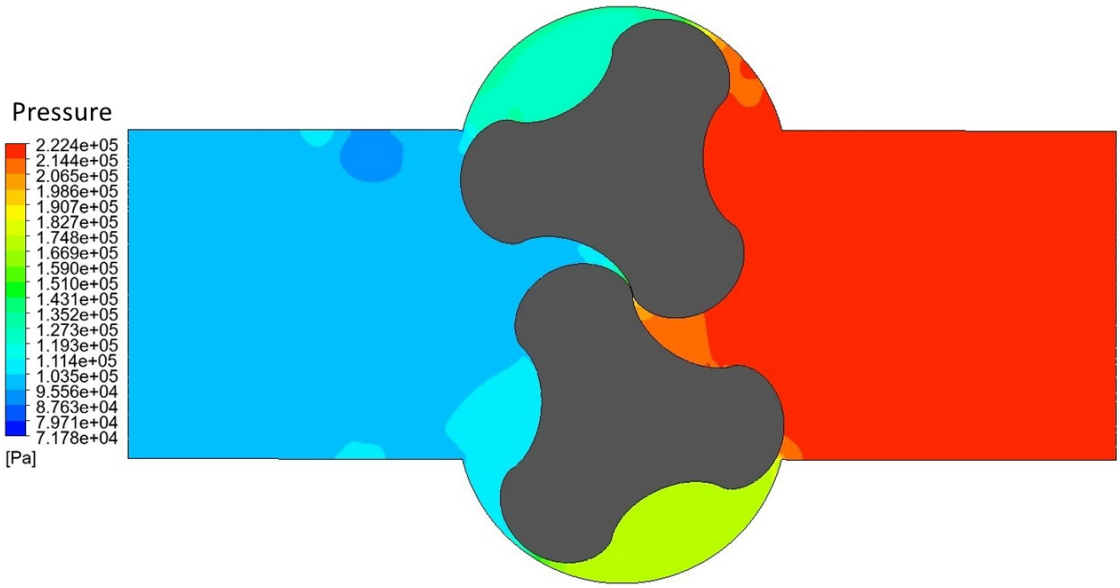

Figure 3.9: Contour of pressure profile for 100 RPM

At 100 RPM, the pressure distribution within the pump exhibits subtle changes compared to the lower rotational speeds. While the general characteristics of the pressure landscape remain recognizable, certain areas, especially in proximity to the lobes, start to display slightly elevated pressures. Even at this moderately increased speed, the lobes' rotation introduces more pronounced interactions with the fluid, leading to localized pressure enhancements. This heightened pressure near the lobes suggests greater fluid compression and possible turbulent effects induced by the

lobe dynamics. The pressure tends to stabilize outside these specific zones, largely resembling the patterns observed at the slower 30 and 60 RPM speeds.

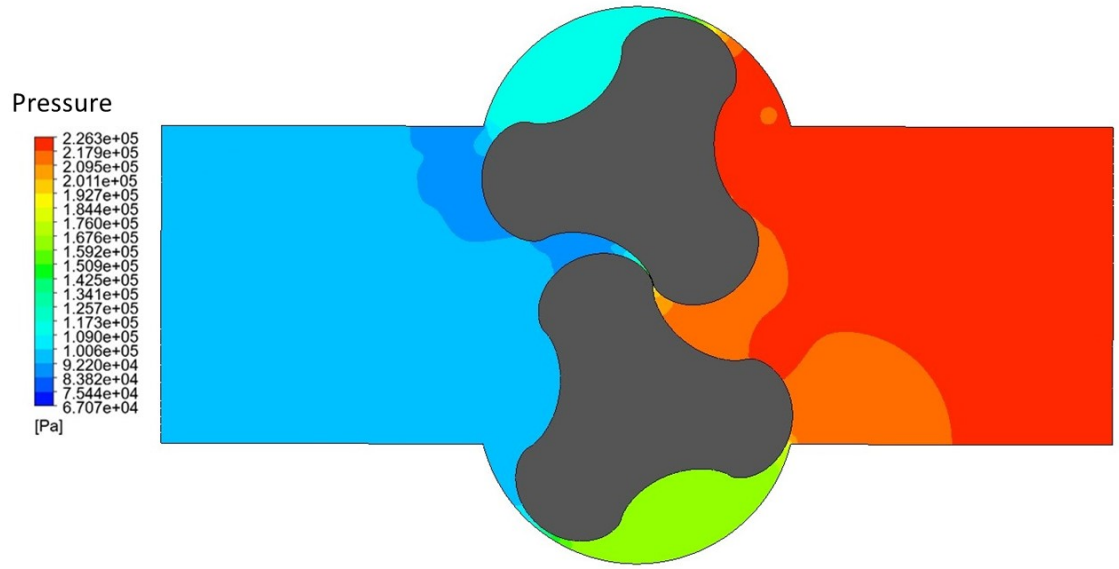

Figure 3.10: Contour of pressure profile for 200 RPM

At 200 RPM, there are differences in the pressure distribution inside the pump. The pressure is notably higher near the lobes, showing the increased impact of the rotating parts on the fluid. As the lobes move, they press the fluid more strongly, creating areas of higher pressure close to them. The region between the lobes and the casing also displays varying pressures, indicating more active flow changes in this area. Beyond these high-pressure areas, the distribution is more uniform but with slight differences hinting at the evolving fluid behavior at this speed. This data highlights how the rotational speed can alter the internal pressure conditions of the pump.

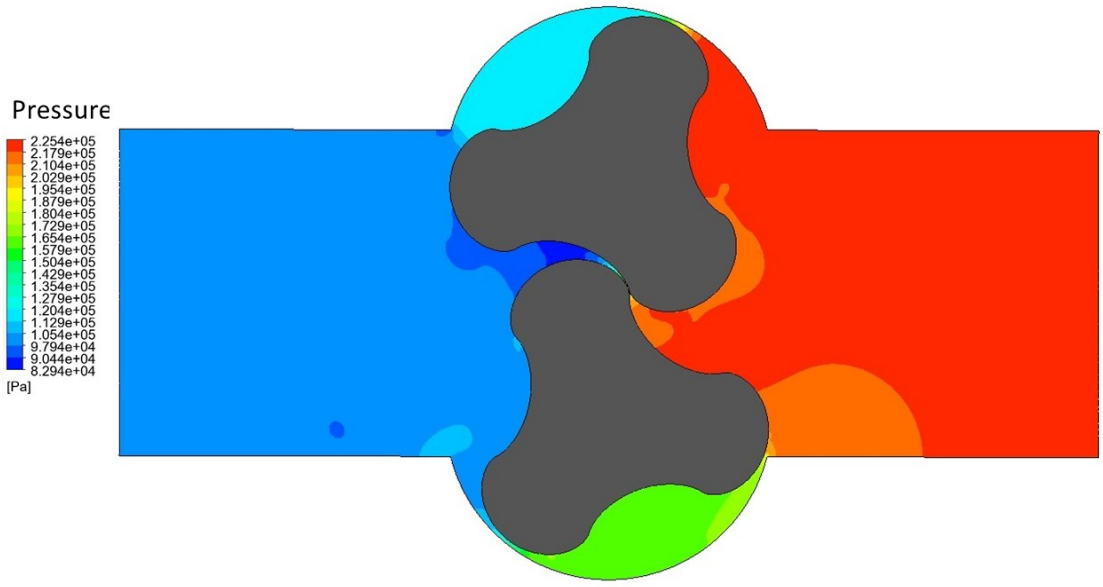

Figure 3.11: Contour of pressure profile for 300 RPM

For the pressure distribution at 300 RPM, the variations in pressure are more pronounced compared to the lower rotational speeds. At the inlet side, there are distinct differences in pressure levels, especially in proximity to the rotating lobes. Similarly, pressure variations are more evident at the outlet side, suggesting that the fluid dynamics at this speed lead to a more diversified pressure environment. The heightened rotational speed influences the pressure distribution across the pump, reflecting the intricate relationship between flow behavior and pressure fields.

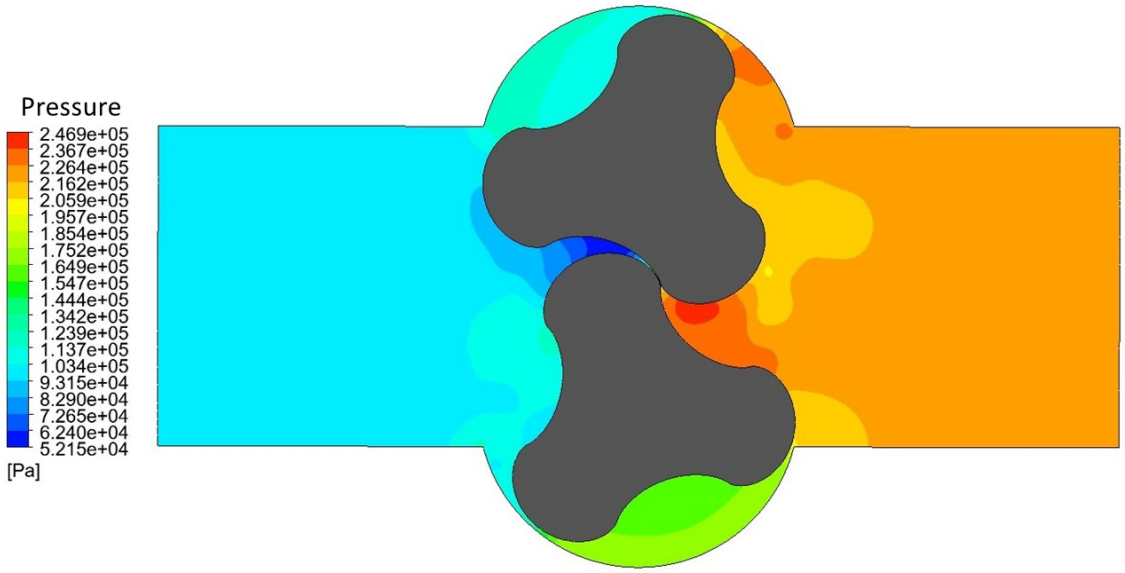

Figure 3.12: Contour of pressure profile for 500 RPM

For the pressure distribution at 500 RPM, there is an increase in the variation of pressure values throughout the pump. One prominent observation is the heightened pressure associated with the regions around the lobes. As the lobes rotate with this higher speed, they seem to induce areas of increased pressure. These amplified pressure variations contrast with the more uniform distributions seen at lower rotational speeds and emphasize the lobes' motion on the internal pressure environment of the pump. This pattern suggests that as the pump's rotational speed increases, the dynamic effects, particularly those due to the lobes, play a more pronounced role in shaping the internal pressure landscape.

Concluding the analysis of pressure distributions at varying rotational speeds, it becomes evident that the lobe pump's operational speed significantly influences the pressure environment within the pump. These variations provide insight into the pump's mechanical performance and hint at marine life's potential interactions and experiences navigating these varying pressure zones.

3.3.3 Residuals

The final part of the results section focuses on residuals to verify the computational model used in this study. Residuals offer a measure for evaluating the reliability and accuracy of the simulations, ensuring that the findings related to velocity profiles, streamlines, and pressure distributions are scientifically meaningful and reliable. The RMS residuals for a rotational speed of 30 RPM are presented in Figure 3.13.

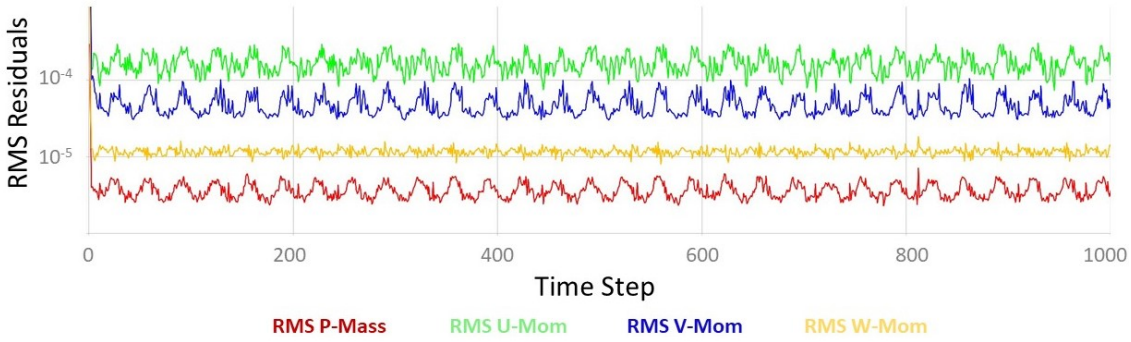

Figure 3.13: RMS residuals for 30 RPM

The convergence criterion for the RMS residuals of 10^{-4}. It should be noted that the RMS U-Mom value was marginally above this value. Despite this slight variation, the RMS residuals displayed consistent behavior across all simulations. Given this, only the residuals corresponding to the 30 RPM case are presented in this subsection. The remaining cases show comparable residual trends, ensuring a robust and reliable simulation.

3.4 Analyzing the Findings: Discussion

Building upon the results, the following discussion aims to provide a deeper understanding of these outcomes. Beginning with the verification and validation, the reliability of the results is ensured. Next, the lobe pump's performance at different rotational speeds will be discussed. Following is a discussion of the impact of the pump's operation on marine life, followed by a balancing of mechanical performance and ecological responsibility. To conclude the discussion, the relevance of the findings is presented, followed by the study's limitations.

3.4.1 Verification and Validation

Verification was used to ensure the model behaves as expected and accurately represents the real-world processes it aims to simulate. The model responded well to changes in rotational speed. When the RPM changed, the model behaved in ways that made sense, indicating that its foundational settings and parameters were correct. This gives confidence in the obtained results.

The monitored RMS residuals generally remained below the set limit, except the RMS U-Mom values, which were slightly above 10^{-4}. Even with this minor deviation, the overall low values indicate that the model reached a stable solution, essential for trustworthy results.

A grid independence study confirmed the model's choice of a 1.5 mm mesh size. This study showed that the chosen mesh size was the right balance between computational time and result accuracy. In other words, making the mesh finer wouldn't significantly change the results, showing that the model is dependable and stable at this level of detail. In conclusion, the verification points to a reliable and robust solution. While simulations always have some inherent limitations, the verification gives reason to trust the outcomes of this study.

Validation ensures that the simulations closely replicate real-world behavior. A challenge faced in this study was the absence of validation data, making it harder to compare the results with experimental or observational results directly. Further complicating matters, any available comparable data from simulations is in 3D, which is not fully comparable to the 2D model in this study. Nevertheless, the 2D model's behavior appeared reasonable and consistent with general fluid dynamics principles, providing some degree of confidence in the outputs.

However, to elevate the credibility of the findings in this study, it would be prudent to develop a 3D

model in future research efforts. A 3D model would offer a more direct and meaningful comparison with available data sets, thus enhancing the validation process. Until then, the 2D model in this study provides insightful preliminary findings while acknowledging the inherent limitations in its scope and advocate for a comprehensive 3D analysis to build upon this foundation.

3.4.2 Lobe Pump Performance

As observed from the simulations, the lobe pump's performance exhibits pronounced variations across different rotational speeds. Particularly at the lower end, with rotational speeds like 30 and 60 RPM, fluid dynamics inside the pump present a calm scene. These speeds show smooth velocity profiles, an attribute suggesting efficient flow with minimal energy loss. Moreover, there is a noticeable absence of disturbances in streamline patterns, implying a reduced likelihood of turbulent flow or areas of stagnation that might influence the pump's performance.

The fluid's behavior inside the pump transforms when transitioning to higher rotational speeds, specifically around the 200 RPM mark and beyond. This change is most evident in the velocity profiles, which show a marked increase in fluid mixing. This heightened mixing introduces complexities; the streamline patterns, previously smooth and more linear, begin exhibiting greater fluctuations, suggesting a transition from laminar to potentially turbulent or transitional flow regimes. These observations raise questions about the pump's efficiency at these higher RPMs and whether such a state of operation might introduce mechanical or operational challenges.

Further insight into the pump's efficiency comes from examining the pressure distributions at the different RPMs. In the calmer operational environments of lower RPMs, the pressure within the pump seems almost undisturbed. It predominantly adheres to the inlet and outlet pressures set for the simulation; a scenario stat might hint at a steady, consistent flow. Yet, at higher RPMs, there are more complicated patterns. The variations in pressure become more pronounced, especially at speeds like 200 RPM. These disparities in pressure can be viewed as indications of a more turbulent flow within the pump.

At 300 RPM, the fluid dynamics within the pump reveal a distinct pattern. Immediately adjacent to the no-slip walls, the fluid is stationary; however, just away from this boundary, the fluid velocity is observed to be the highest, creating a layer that seems to move along the contour of the pump walls. In contrast, the central regions display a predominant circular motion, possibly hinting at vortex formation. The interactions between the rotating lobes and the fluid likely influence this behavior. The elevated momentum, due to the increased rotational speed, brings about noticeable changes in the fluid's behavior, highlighting the pronounced effect that rotational speed has on the internal fluid dynamics of the pump.

At 500 RPM, the lobe pump's internal dynamics suggest a significant transformation in flow behavior. The dominant circular streamlines observed, particularly at the inlet and outlet regions, reflect a considerable conversion of the pump's rotational energy into fluid motion. However, this transformation might come at a cost. The increased velocities observed, combined with the evident swirling patterns, could hint at the onset or strengthening of turbulence. Turbulence, while advantageous in certain scenarios for its mixing capabilities, often reduces the energy efficiency of fluid systems. This turbulent behavior might lead to energy losses due to chaotic fluid structures and vortex shedding. Consequently, despite the apparent boost in flow rates at 500 RPM, the emerging turbulence might mean that this is not the optimal speed for energy-efficient pump operation. This observation underscores the need to consider both flow characteristics and energy considerations when determining the ideal operating RPM for the pump.

The fluid dynamics inside the pump have ramifications on its mechanical components. Smooth, predictable flow patterns might correlate with reduced wear and tear, potentially leading to extended component life and reduced maintenance needs. In contrast, regions of turbulent flow or pronounced velocity gradients could accelerate the wear on the pump's internals.

To sum up the results regarding pump performance, it can be seen at lower RPMs that the pump performs stable and efficiently, but the dynamics grow more intricate with increased rotational speed. Observations from the simulations hint at a potential optimal RPM range that harmonizes

efficiency with diminished mechanical wear. This optimal range can be approximated by analyzing the pump's behavior across various RPMs. However, for a precise determination, additional simulations and in-depth analysis would be essential.

3.4.3 Analyzing Fish-Friendly Features in Lobe Pump Fluid Dynamics

Protecting fish and marine life is a key concern when designing and using pumps in aquatic environments. While many traditional pumps can harm fish, the unique design of the lobe pump might offer a different experience. This section examines the flow patterns and pressure distributions within the lobe pump, presented in Section 3.3, to identify aspects that may be beneficial or harmful to fish.

Velocity Profiles and Fish Movement

The influence of varying RPMs on the lobe pump's fluid dynamics is multifaceted, encompassing changes in velocity profiles, vortex formations, and potential turbulence emergence. These factors have implications for the pump's operational performance and the movement and safety of fish within the flow.

At the lower rotational speeds of 30 and 60 RPM, the fluid behavior is predominantly calm, characterized by smooth and steady velocity profiles. The streamline patterns are linear, hinting at efficient flow with minimal disturbances. While ideal for pump operations due to reduced wear and potential energy savings, such conditions also bode well for aquatic life. The absence of pronounced vortices and turbulent regions ensures safer transit conditions for fish.

However, a shift is noticeable around 200 RPM. The previously uniform velocity profiles show more pronounced fluctuations, especially at the outlet side of the pump. These deviations and emerging circular flow patterns signal the initial stages of vortex formation. Although not highly intensive at this stage, the changing fluid environment could begin to pose navigational challenges for fish, especially those less adept at maneuvering in swirling currents.

The 300 RPM operational scenario amplifies these trends. Vortex behavior is dominant, evident in velocity profiles and streamline patterns. The fluid's interactions with the pump's geometry and its heightened energy due to increased rotational speed drive these intricate flow patterns. For fish, these pronounced vortices can be zones of potential disorientation, making passage through the pump more challenging.

By 500 RPM, the complexity intensifies further. Mature vortex formations are evident, and the dynamic nature of the velocity profiles suggests the pump is in a turbulent flow regime. Turbulence, characterized by its chaotic and unpredictable motion, can introduce operational challenges such as increased wear, energy inefficiencies, and heightened maintenance demands. These turbulent zones spell heightened danger for aquatic life, presenting erratic flow conditions that can stress, harm, or even be fatal for fish.

The balance between rotational speed, fluid dynamics, and their consequences becomes clear in drawing together these observations. Understanding this balance is pivotal for achieving operational efficiency while ensuring the lobe pump remains safe for aquatic life.

Pressure Dynamics and Fish Safety

The evolution of pressure distributions across different RPMs offers additional dimensions of understanding in assessing the lobe pump's compatibility with fish-friendly operations.

Stable pressures are observed at the foundational rotational speeds, with minor fluctuations. Such environments present minimal external pressure disturbances for fish, ensuring their physiological systems, especially the swim bladders, remain relatively unaffected. The swim bladder, crucial for a

fish's buoyancy, is sensitive to rapid pressure changes. In environments where pressure is consistent, the risk of barotrauma—a physical injury caused by pressure differences—is considerably reduced.

However, as the pump's rotational speed escalates, especially at the 200 and 300 RPM marks, the pressure landscape inside the pump starts to diversify. Variations become more pronounced, suggesting dynamic shifts in the flow behavior and its interactions with the pump's structure. Such quick pressure changes can be unsettling for fish. Frequent and rapid fluctuations can challenge their natural equilibrium, possibly leading to stress or physiological disruptions.

By 500 RPM, the complexities in the pressure profiles peak. The stark pressure contrasts indicate strong interactions between the fluid and the pump's rotating components, especially the lobes. For fish navigating such a setting, adjusting to changing pressures can be tiring and disorienting. Prolonged exposure to such dynamic environments can heighten the risk of injuries and stress, challenging their overall well-being.

In conclusion, while the pressure distributions offer insights into the pump's internal operations, they also underscore the challenges fish might face. Recognizing these pressure-related risks and their implications is pivotal when designing or operating pumps in environments where fish safety is a priority.

Lobe Geometry and Clearance Gap

The design and geometry of the pump's lobes play a pivotal role in determining the nature of fluid flow and, by extension, the experience of aquatic organisms passing through. The contours, sharpness, and surface features of the lobes can influence the pump's efficiency and how fish interact with the structures. In a well-designed lobe pump, sharp or jagged features are minimized or eliminated, as they can pose a direct threat by potentially injuring fish as they navigate the pump. Conversely, smooth, streamlined lobe surfaces are prioritized for multiple reasons. Not only do they reduce the risk to fish, ensuring that they can traverse the pump with minimal physical contact, but smooth surfaces also enhance the pump's performance by reducing flow resistance and promoting efficient fluid movement.

Furthermore, the overall shape and geometry of the lobes influence the creation of pressure zones and flow regions. A well-optimized lobe design can reduce the formation of high-pressure zones or intense vortices, which can be particularly stressful for fish.

The clearance gap is another crucial design element when evaluating the potential impact on fish. This gap is particularly narrow in the lobe pump design under consideration, measuring only around 1 mm. Such a tight clearance can present hazards while not intended for fish passage. Fish, especially smaller ones, might risk getting drawn toward or trapped in this narrow gap due to the fluid dynamics near the lobes. This could potentially result in physical injury to the fish. Furthermore, the clearance gap is critical from a pump performance standpoint as it influences the pump's efficiency by affecting leakage rates. This gap is meticulously calibrated in a well-designed lobe pump to optimize hydraulic performance and minimize adverse effects on aquatic life.

The challenge lies in optimizing the clearance gap for pump performance and fish welfare. A gap conducive to fish movement might not always align with the optimal design for pump efficiency. Designers must consider trade-offs, possibly looking at adjustable geometries or adaptive designs catering to performance and ecological considerations.

In conclusion, while the primary purpose of the lobe pump's design is fluid transport, it is imperative to consider the biological implications of design choices. The geometry of the lobes and the clearance gap can significantly impact fish health and survival, underlining the importance of a pump design that considers both mechanical and ecological aspects.

Finding the Optimal Rotational Speed for Pump Operation and Aquatic Safety

Firstly, when considering the lobe pump's performance, it is evident that its performance and fluid behavior vary significantly across different rotational speeds. Rotational speeds of 30 and 60 RPM display calm fluid dynamics characterized by smooth velocity profiles and streamlined patterns. This calm behavior suggests efficient pump operation with potential energy savings and ensures safer transit conditions for aquatic life. At these rotational speeds, the environment within the pump appears to be gentle, with reduced turbulent zones and vortex formations, making it more conducive for fish movement.

However, as the rotational speed increases to around 200 RPM and beyond, vortices start to form, and the behavior of the fluid suggests a transition towards a turbulent regime, especially at the 500 RPM mark. While higher RPMs may yield enhanced flow rates and operational capacities, they present challenges. These include potential wear and tear on the pump's components, energy inefficiencies, and a heightened risk for aquatic inhabitants due to erratic and possibly harmful flow conditions.

ALPHEUS's chosen operational RPM range is set between 30 to 60 RPM. This choice seems suitable based on the simulations and observations from this study. It seems to balance ensuring optimal pump performance and safeguarding aquatic life. The lower RPM range reduces the likelihood of turbulent flow and related mechanical challenges. It prioritizes the welfare of marine life, reducing potential harm and stress to the fish passing through. Nevertheless, based on the relatively stable fluid dynamics observed slightly beyond this range, it is reasonable to consider that rotational speeds up to 100 RPM can also be suitable, though with a more careful evaluation of the trade-offs involved.

3.4.4 Relevance of the Results

This study aims to add to the existing fluid dynamics knowledge, specifically in marine applications like the ALPEHUS project. Offering an exploration of key parameters such as velocity profiles, streamline patterns, and pressure distributions at varied operational speeds, the findings should be viewed as a foundational step for more detailed future research.

The ecological implications are another area to which this study aims to contribute. The insight into how varying flow characteristics could affect aquatic life suggests possible avenues for optimizing lobe pump designs. This is particularly important for environmentally sensitive projects like ALPEHUS, which aim to balance technological efficacy with ecological sustainability.

Finally, while the data from this study are preliminary, they may be useful for future regulatory considerations and environmental assessments, especially those related to marine pumped hydro storage initiatives like ALPHEUS. As the drive for sustainable engineering solutions continues, the environmental impact of technologies like lobe pumps remains a critical area for research. In this light, this study hopes to offer a small but meaningful step towards a future where engineering and ecology can coexist more harmoniously.

3.4.5 Limitations

The study offers valuable insights but has several limitations that must be acknowledged for a comprehensive understanding of the results.

- The use of 2D simulations: Real-world fluid dynamics are inherently 3D, and a 2D study may not fully capture the complex flow patterns or their impact on fish.
- 1 mm clearance gap: This assumption could significantly affect the pressure and velocity profiles and how fish interact with the pump.

- Simulations performed in pump mode: The lobe pump will also function as a turbine in actual applications. This limitation could mean that the findings are not fully representative of all operational states that the pump will experience.
- Mesh quality: Some elements exhibited poor aspect ratios, which could compromise the simulation accuracy, particularly in capturing boundary layer effects and flow separation regions.
- Absence of comparable results: Made the validation process challenging, which could affect both the results and the conclusions.
- Additional study limitations include various model simplifications, such as neglecting factors like heat transfer. The study also did not account for static environmental conditions like temperature. Moreover, while the focus was on the mechanical aspects of the pump's operation, biological consequences like stress or longer-term health effects on fish were not considered.

While the findings of this study offer insights into the fluid dynamics of lobe pumps and their potential impact on aquatic life, they are subject to several limitations. Acknowledging these constraints underscores the areas where the study could be improved and outlines avenues for future research to provide a more comprehensive and nuanced understanding of the topic.

Chapter 4

Conclusion

This master's thesis has studied the fluid flow behavior in a three-lobe pump with epicycloidal lobes using CFD simulations. The objective was to understand how the pump works and how it might affect marine life, especially fish.

The simulations, using a structured mesh with an element size of 1.5 mm and supplemented by inflation layers, provided detailed insights into the pump's behavior under varied rotational speeds. The adaption of the SST $k-\omega$ turbulence model and the Immersed Boundary Method played an important role in this analysis. A clear pattern emerged from the results, indicating that rotational speeds from 30 to 100 RPM create smooth flows and minimal turbulence. These rotational speeds create an environment that appears not to harm or disturb the well-being of aquatic life, particularly fish.

However, the situation changes when the rotational speed reaches 200 RPM. The pump introduces pronounced turbulent flows and distinct vortex formations at this speed. Such turbulence and vortices are not merely a mechanical concern but also represent a significant hazard for marine life, especially fish. Instead of facilitating a smooth water flow conducive to aquatic creatures, the pump seems to divert energy toward generating these chaotic patterns. This compromises its performance and elevates the risks for the marine inhabitants.

The study underscores the importance of finding a balance by considering both the ecological factors and the mechanical performance. The ALPHEUS project's decision to operate the lobe pump within the 30 to 60 RPM bandwidth emerges as a sound one, reaching for both efficiency and fish-friendliness.

In summation, the findings of this thesis underscore that, up to approximately 100 RPM, the pump can be deemed fish-friendly, creating favorable conditions for marine life. As marine engineering industries evolve, striking the right balance between operational efficiency and ecological conservation remains critical.

Chapter 5

Further work

While the current study provides valuable insights into the fluid dynamics of lobe pumps and their impact on fish, several aspects remain open for further study.

The major area for further work is the use of 3D simulations. This study employed 2D simulations for reasons of computational efficiency. However, a 3D model could provide a more accurate representation of complex flow patterns.

While this study has concentrated on the pump mode of operation, it is important to note that the pump is also planned to operate as a turbine in its intended seawater application. Therefore, the impact of turbine mode on fish warrants investigation in future research. Additionally, the transitional states between pump and turbine modes, as well as the pump's start-up or shut-down phases, deserve further study. Exploring these transitions could offer a more complete understanding of the pump's overall impact on fish.

One area that has not been adequately covered in this study is the impact of turbulence. The current study only assumed the presence of turbulence when evaluating flow patterns. A more detailed investigation into turbulence levels would be beneficial, especially to understand its potential effects on fish.

Another aspect that should be considered in further work is the size of the fish being transported. Different fish sizes could yield different interactions with fluid flow and turbulence. For example, smaller fish may face a higher risk of becoming trapped in gaps within the pump, a potentially significant concern. It's also crucial to note that this study approached the topic from a mechanical viewpoint. For a more holistic understanding, future research should include a biological perspective, investigating factors such as stress levels, scale damage, or swim bladder injuries in fish. The material properties of the pump could also be studied to ascertain their impact on fish well-being.

By addressing these areas, future work could provide a more nuanced and comprehensive understanding of how lobe pump operation in seawater would affect the surrounding aquatic life, especially fish.

Bibliography

[1] Boer WW, Verheij FJ, D Z, R D. The Energy Island - An Inverse Pump Accumulation Station; 2007.

[2] Hoffstaedt JP, Truijen D, Fahlbeck J, Gans LHA, Qudaih M, Laguna AJ, et al. Low-head pumped hydro storage: A review of applicable technologies for design, grid integration, control and modelling. Renewable and Sustainable Energy Reviews. 2022;158:112119.

[3] Kang YH, Vu HH, Hsu CH. Factors impacting on performance of lobe pumps: a numerical evaluation. Journal of Mechanics. 2012;28(2):229-38.

[4] Hestetræet M. Numerical setup for a positive displacement reversible pump-turbine machine; 2023.

[5] Aissa MH, Verstraete T, Vuik C. Use of modern GPUs in design optimization. In: The 10th ASMO UK/ISSMO conference on Engineering Design Optimization Product and Process Improvement; 2014. p. 1-2.

[6] Jacoby R. When to Use a Positive Displacement Pump. Pump School com, Viking Pump, Inc, www pumpschool com. 2002.

[7] Dick C, Puchta M, Bard J. StEnSea - Results from the pilot test at Lake Constance. Journal of Energy Storage. 2021;42:103083.

[8] Puchta M, Bard J, Dick C, Hau D, Krautkremer B, Thalemann F, et al. Development and testing of a novel offshore pumped storage concept for storing energy at sea- Stensea. Journal of Energy Storage. 2017;14:271-5.

[9] Hahn H, Hau D, Dick C, Puchta M. Techno-economic assessment of a subsea energy storage technology for power balancing services. Energy. 2017;133:121-7.

[10] Rehman S, Al-Hadhrami LM, Alam MM. Pumped hydro energy storage system: A technological review. Renewable and Sustainable Energy Reviews. 2015;44:586-98.

[11] Alpheus. About the project; 2022. Available from: https://alpheus-h2020.eu/about/.

[12] Sultan IA, Phung TH. Positive displacement machines: modern design innovations and tools. Academic Press; 2019.

[13] Sonawat A, Kim SJ, Yang HM, Choi YS, Kim KM, Lee YK, et al. Positive displacement turbine-A novel solution to the pressure differential control valve failure problem and energy utilization. Energy. 2020;190:116400.

[14] Krampe P, Ørke PR. Four-Quadrant Operation of Rotary Lobe Pumps and Regenerative Throttling. International Rotating Equipment Conference; 2012. .

[15] Hesse J. Structured meshes and reliable CFD simulations: TwinMesh for positive displacement machines.

[16] Schiffer J. A comparison of CFD-calculations and measurements of the fluid flow in Rotating Displacement Pumps. International Rotating Equipment Conference; 2012. .

[17] Kovacevic A, Rane S. Challenges in 3D CFD Modelling of Rotary Positive Displacement Machines. In: Journal of Physics: Conference Series. vol. 1909. IOP Publishing; 2021. p. 012063.

[18] Kim H, Marie H, Patil S. Two Dimensional Cfd Analysis Of A Hydraulic Gear Pump. In: 2007 Annual Conference & Exposition; 2007. p. 12-1506.

[19] Cavazzini G, Giacomel F, Benato A, Nascimben F, Ardizzon G. Analysis of the inner fluid-dynamics of scroll compressors and comparison between CFD numerical and modelling approaches. Energies. 2021;14(4):1158.

[20] Prakash M, Stokes N, Bertolini J, Tatford O, Gomme P. SPH simulations of a lobe pump: prediction of protein shear stress at different pump efficiencies. In: Proc: 3rd Int. Conf. on CFD in Minerals and Process Industries; 2003. p. 183-8.

[21] Munih J, Hočevar M, Petrič K, Dular M. Development of CFD-based procedure for 3d gear pump analysis. Engineering Applications of Computational Fluid Mechanics. 2020;14(1):1023-34.

[22] Papes I, Degroote J, Vierendeels J. 3D CFD analysis of an oil injected twin screw expander. In: ASME International Mechanical Engineering Congress and Exposition. vol. 56284. American Society of Mechanical Engineers; 2013. p. V06AT07A040.

[23] Gans LHA, Storli PTS. Multidisciplinary optimized PD design; 2022.

[24] Khalili M, Larsson M, Müller B. Immersed boundary method for the compressible Navier-Stokes equations using high order summation-by-parts difference operators. In: Progress in Applied CFD–CFD2017 Selected papers from 12th International Conference on Computational Fluid Dynamics in the Oil & Gas, Metallurgical and Process Industries. SINTEF akademisk forlag; 2017. .

[25] Bardina JE, Huang PG, Coakley TJ. Turbulence modeling validation, testing, and development; 1997.

[26] Versteeg HK, Malalasekera W. An introduction to computational fluid dynamics: the finite volume method. Pearson education; 2007.

[27] Menter FR. Improved two-equation k-omega turbulence models for aerodynamic flows; 1992.

[28] Menter FR, Kuntz M, Langtry R. Ten years of industrial experience with the SST turbulence model. Turbulence, heat and mass transfer. 2003;4(1):625-32.

[29] Hoffstaedt J, Jarquín-Laguna A, Fahlbeck J, Nilsson H. System model development and numerical simulation of low-head pumped hydro storage. Trends in Renewable Energies Offshore. 2022:757-63.

[30] Levy D, Chaffin M. Comparison of viscous grid layer growth rate of unstructured grids on CFD drag prediction workshop results. In: 28th AIAA Applied Aerodynamics Conference; 2010. p. 4671.

[31] Knupp PM. Algebraic mesh quality metrics. SIAM journal on scientific computing. 2001;23(1):193-218.

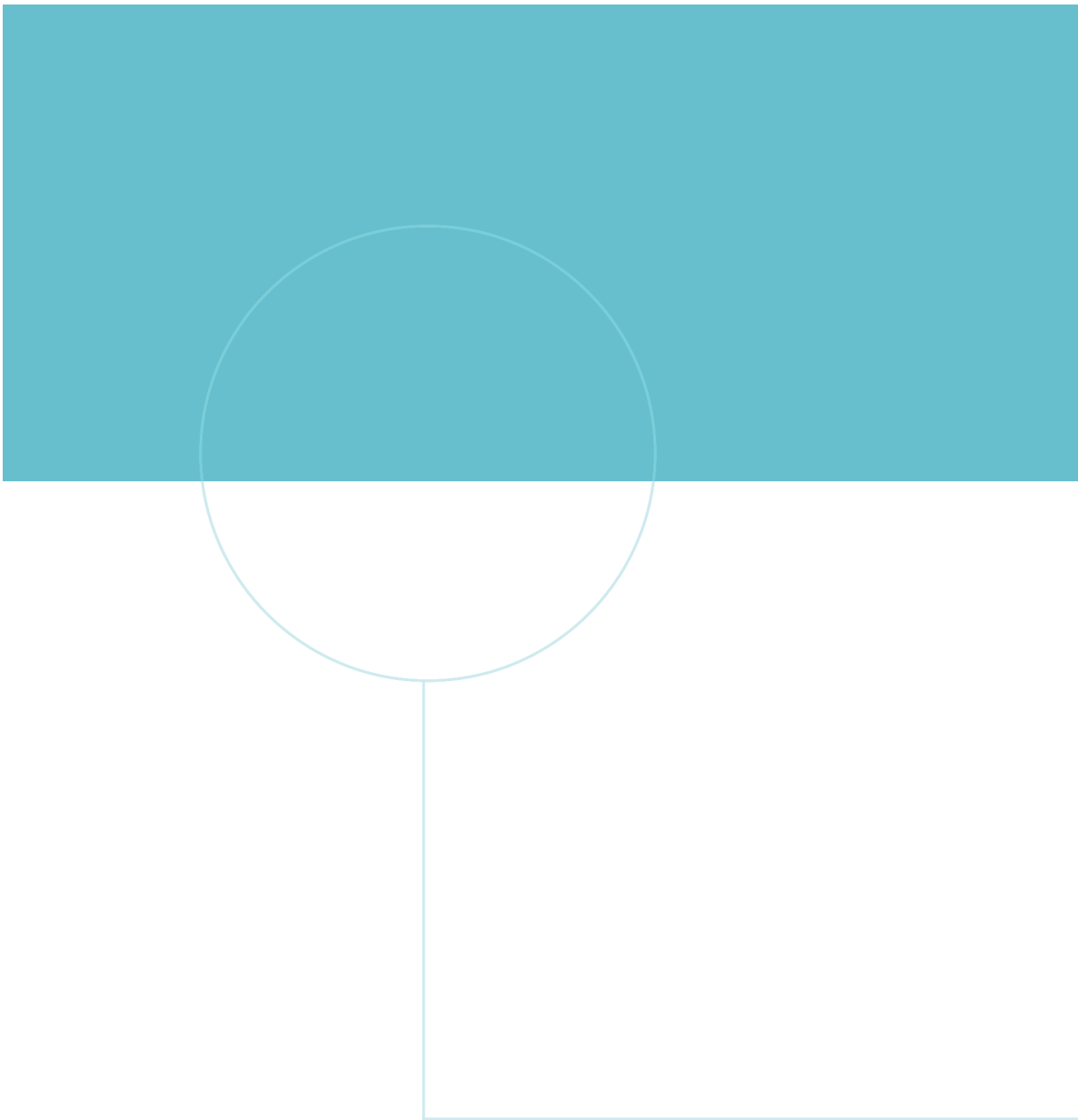

NTNU

Kunnskap for en bedre verden